OXFORD

Cerebral Cortex, 2023, **33**, 3401–3420
https://doi.org/10.1093/cercor/bhac280
Advance access publication date 19 July 2022
Original Article

Estrogens rapidly shape synaptic and intrinsic properties to regulate the temporal precision of songbird auditory neurons

Garrett B. Scarpa[1], Joseph R. Starrett[1], Geng-Lin Li[2], Colin Brooks[1], Yuichi Morohashi[3], Yoko Yazaki-Sugiyama[3], Luke Remage-Healey[1,*]

[1]Neuroscience and Behavior, Center for Neuroendocrine Studies, University of Massachusetts, 639 N. Pleasant St., Amherst, MA 01003, United States,
[2]Department of Otorhinolaryngology, Eye and ENT Hospital, Fudan University, 83 Fenyang Rd, Xuhui District, Shanghai 200031, China,
[3]Okinawa Institute of Science and Technology (OIST) Graduate University, 1919-1 Tancha, Onna, Kunigami District, Okinawa, Japan

*Corresponding author: Neuroscience and Behavior, Center for Neuroendocrine Studies, 212 Morrill Science Center IVN, University of Massachusetts, Amherst, MA 01003, United States. Email: healey@cns.umass.edu

Sensory neurons parse millisecond-variant sound streams like birdsong and speech with exquisite precision. The auditory pallial cortex of vocal learners like humans and songbirds contains an unconventional neuromodulatory system: neuronal expression of the estrogen synthesis enzyme aromatase. Local forebrain neuroestrogens fluctuate when songbirds hear a song, and subsequently modulate bursting, gain, and temporal coding properties of auditory neurons. However, the way neuroestrogens shape intrinsic and synaptic properties of sensory neurons remains unknown. Here, using a combination of whole-cell patch clamp electrophysiology and calcium imaging, we investigate estrogenic neuromodulation of auditory neurons in a region resembling mammalian auditory association cortex. We found that estradiol rapidly enhances the temporal precision of neuronal firing via a membrane-bound G-protein coupled receptor and that estradiol rapidly suppresses inhibitory synaptic currents while sparing excitation. Notably, the rapid suppression of intrinsic excitability by estradiol was predicted by membrane input resistance and was observed in both males and females. These findings were corroborated by analysis of in vivo electrophysiology recordings, in which local estrogen synthesis blockade caused acute disruption of the temporal correlation of song-evoked firing patterns. Therefore, on a modulatory timescale, neuroestrogens alter intrinsic cellular properties and inhibitory neurotransmitter release to regulate the temporal precision of higher-order sensory neurons.

Key words: aromatase; neuromodulation; cortex; zebra finch; learning; estradiol.

Introduction

Shifts in social and environmental contexts can drive changes in the response properties of sensory neurons. Neuromodulators like dopamine, serotonin, and oxytocin can signal transient changes in context and thereby modify sensory networks and intrinsic properties (Vogels and Abbott 2009; Marlin et al. 2015; Kuchibhotla et al. 2017; Gentile Polese et al. 2021). Similarly, estrogens are locally synthesized in many regions of the brain, and they can act as acute neuromodulators of circuits and behavior ("neuroestrogens"). The capacity for neuroestrogen synthesis, most prominently the expression of the synthesis enzyme aromatase, is particularly enriched in regions associated with sensory processing and neural plasticity, including the temporal cortex of humans (Yague et al. 2006; Azcoitia et al. 2011), the auditory forebrain of songbirds (Schlinger and Arnold 1993; Saldanha et al. 2000, 2013; De Groof et al. 2017; Ikeda et al. 2017), as well as the hippocampus and hypothalamus of many vertebrate species (Callard et al. 1977; Beyer et al. 1994; Winkler and Wade 1998; Saldanha et al. 2000; Forlano et al. 2001, 2006; Balthazart and Ball 2006; Cornil 2009; Fester et al. 2009; Balthazart et al. 2018). The enzymatic activity of aromatase—and resultant local neuroestrogen levels—can also fluctuate rapidly in some brain regions in response to sensory inputs, physiological changes, and social contexts (Balthazart et al. 2006; Remage-Healey et al. 2008; Cornil 2009; Kenealy et al. 2013; Chao et al. 2015; Sato and Woolley 2016). In turn, estrogens such as 17-beta-estradiol (E2) can have rapid (i.e. within minutes) effects on neuronal firing in many brain areas (Wong and Moss 1992; Smith et al. 2002; Remage-Healey 2004; Remage-Healey and Bass 2007; Meitzen et al. 2012; Rudolph et al. 2016; Hedges et al. 2018; Soutar et al. 2022).

The functional outcomes of rapid neuroestrogen signaling include enhanced coding and gain of auditory forebrain neurons in adult and juvenile songbirds (Remage-Healey et al. 2010; Remage-Healey and Joshi 2012; Vahaba et al. 2017; Krentzel et al. 2018). Suppressing neuroestrogen synthesis can disrupt the formation of new auditory memories (Macedo-Lima and Remage-Healey 2020) as well as spatial memories (Bailey and Saldanha 2015; Tuscher et al. 2016) and other cognitive functions (Kokras et al. 2018; Gervais et al. 2019;

Received: June 8, 2022. **Revised:** June 20, 2022. **Accepted:** June 22, 2022

Lu et al. 2019). Therefore, like other neuromodulators, neuroestrogens can modulate neurophysiology and behavior in a variety of species and brain regions.

Despite this extensive literature, it is not yet clear what synaptic and intrinsic mechanisms account for the effects of estrogens on cognitive and sensory representations. A large, parallel body of work has shown that E2 can shape synaptic and intrinsic physiology in the hypothalamus, striatum, and hippocampus (Kelly and Ronnekleiv 2009; Roepke et al. 2011; Moenter and Chu 2012; Oberlander and Woolley 2016; Jain et al. 2019; Proaño et al. 2020) and that E2 can alter synaptic strength in the hippocampus (Kramar et al. 2009; Srivastava et al. 2011; Huang and Woolley 2012; Lu et al. 2019). The rapid actions of E2 on neuronal physiology involve a host of cellular and current targets. In GnRH neurons alone, E2 can rapidly regulate retrograde nitric oxide signaling (Farkas et al. 2018), phosphorylation of cAMP response element-binding protein (Kwakowsky et al. 2012), potentiation of a slow afterdepolarization sodium current (Chu and Moenter 2006), and suppression of a calcium-activated potassium current that governs afterhyperpolarization (Chu et al. 2009; Moenter and Chu 2012). In hippocampal neurons, E2 potentiates a kainate-induced current (Gu and Moss 1998) as well as L-type calcium channels (Jain et al. 2019) to increase excitability. In neurons of the ventromedial hypothalamus, E2 regulates voltage-gated calcium channels (Lee et al. 2008) as well as both inward sodium and outward potassium currents (Kow et al. 2006) to increase excitability. Cell-line experiments have also identified the acute regulation of 2-pore potassium channels by membrane estrogen receptor activation (Choudhury and Sikdar 2018). With this plenteous knowledge about the rapid actions of E2 on neurons (reviewed in: Moenter and Chu 2012; Kow and Pfaff 2018; Vail and Roepke 2019; Stincic and Kelly 2022), there is now an opportunity to directly connect the acute effects of estrogens on synaptic and intrinsic physiology of neurons with cognitive- and sensory-dependent behaviors.

Here, we use a combination of whole-cell patch clamp recordings and calcium imaging to begin to understand the synaptic and intrinsic mechanisms of acute neuroestrogen regulation of auditory neurons in the songbird forebrain. We focus on the higher-order auditory region NCM (caudomedial nidopallium) that is characterized by dense aromatase expression (Saldanha et al. 2000; Ikeda et al. 2017) and is a prominent site of auditory recognition memory and auditory learning (Dong and Vicario 2020; Macedo-Lima and Remage-Healey 2020; Theilman et al. 2021). Our experiments demonstrate rapid E2-dependent regulation of both intrinsic and synaptic properties of NCM neurons that together contribute to their temporal firing precision. These findings provide insights into a key neuromodulatory mechanism that supports the encoding and representation of highly dynamic sensory stimuli.

Materials and methods

Subjects

All procedures were conducted in accordance with University of Massachusetts Amherst IACUC guidelines. Adult male and female zebra finches (*Taeniopygia guttata*) were obtained from commercial suppliers or from our laboratory breeding colony. Ex vivo whole-cell slice recordings generally followed established procedures in our laboratory (Caballero et al. 2019; Gervais et al. 2019; Macedo-Lima et al. 2021; Spool et al. 2021). Here, we recorded from 73 cells ex vivo derived from 64 birds, as outlined below. For current-clamp experiments, analyses included 13 cells from 12 males and 5 cells from 5 females that were exposed to 50 nM E2, 5 cells from 4 males exposed to 50 nM E2 in the presence of G36 (an antagonist to the G-protein coupled estrogen receptor1; GPER1), and 3 cells each from 3 males and 3 females that were used for rundown controls. For voltage clamp experiments, we analyzed 13 cells from 10 males and 13 cells from 11 females that were exposed to 50 nM E2, 2 cells each from 1 male and 1 female that were exposed to 100 nM E2, and 7 cells from 7 females and 4 cells from 4 males that were used for rundown controls. As described below, calcium imaging experiments were performed with zebra finches that were virally transduced to express GCaMP6f restricted to GABAergic neurons. For these, we analyzed 288 units from 3 separate slices from 1 female that were exposed to E2. We also recorded a number of untreated units from 1 male at a high sampling rate using line-scanning methods, in order to confirm detection of fast, action potential (AP)-like calcium transients. For the in vivo recording experiments, we examined data from 12 isolated single units from 5 birds ($n = 3$ males, 2 females).

Solutions

Across all experiments, solutions were prepared using high resistivity (>18 MΩ), double-distilled water (ddH_2O) and high purity salts. A glycerin-based external cutting solution (substituting for NaCl and sucrose) was used for all experiments, except for those utilizing the voltage clamp configuration, to improve slice survival time (Ye et al. 2006). Because electrophysiological properties of NCM neurons can shift initially upon break-in (Dagostin et al. 2015), we allowed each cell to recover for a minimum of 5 min following break-in, and at least 8 min of baseline data were subsequently collected from each neuron.

The sucrose-based cutting solution used for voltage clamp recordings contained (in mM): 112 NaCl, 25 $NaHCO_3$, 2.5 KCl, 1.25 NaH_2PO_4, 0.5 $CaCl_2$, 7 $MgCl_2 \bullet 6H_2O$, 25 dextrose, 75 sucrose, 0.4 ascorbic acid, 2 sodium pyruvate, 3 myo-inositol; 354 mOsm/kg H_2O; pH 7.4 when saturated with 95% O_2/5% CO_2. The glycerin-based cutting solution that we used for all other experiments contained (in mM): 222 glycerin, 25 $NaHCO_3$, 2.5 KCl,

1.25 NaH_2PO_4, 0.5 $CaCl_2$, 3 $MgCl_2 \bullet 6H_2O$, 25 dextrose, 0.4 ascorbic acid, 2 sodium pyruvate, 3 myo-inositol; 310 mOsm/kg H_2O; pH 7.4 when saturated with 95% O_2/5% CO_2. The aCSF external solution contained (in mM): 111 NaCl, 25 $NaHCO_3$, 2.5 KCl, 1.25 NaH_2PO_4, 2 $CaCl_2$, 1 $MgCl_2 \bullet 6H_2O$, 25 dextrose, 0.4 ascorbic acid, 2 sodium pyruvate, 3 myo inositol; 310 mOsm/kg H_2O; pH 7.4 when saturated with 95% O_2/5% CO_2. For voltage clamp experiments examining miniature inhibitory postsynatpic currents (mIPSCs), a cesium-based internal solution contained (in mM): 139 CsCl, 8 NaCl, 10 TEACl, 0.2 EGTA, 10 HEPES, 2 MgATP, 0.2 NaATP; 290–310 mOsm/kg H_2O; pH 7.3. For current-clamp experiments and voltage clamp experiments examining miniature excitatory postsynaptic currents (EPSCs), a potassium-based internal solution contained (in mM): ~100 potassium gluconate, 20 KCl, 0.1 $CaCl_2$, 5 HEPES, 5 EGTA, 3 Mg-ATP, 0.5 Na-GTP, 20 $C_4H_8N_3O_5PNa_2 \bullet 4H_2O$; 290–305 mOsm/kg H_2O; pH 7.4. Post-recording, tissue sections were drop-fixed in 4% paraformaldehyde dissolved in 0.025 M phosphate buffer (PB), then stored at −20 °C in a cryoprotectant solution composed of 30% sucrose, 30% ethylene glycol, and 1% polyvinylpyrrolidone in 0.1 M PB.

Pharmacological agents

DNQX, bicuculline, and tetrodotoxin citrate (TTX citrate) were purchased from Tocris Biosciences, E2 from Alfa Aesar, G1 from Azano Scientific, G36 from both Azano Scientific and Cayman Chemical, and fadrozole from Novartis. E2 was reconstituted in 100% ethanol (EtOH), then diluted in ddH_2O. DNQX, bicuculline, and G36 were all diluted in dimethyl sulfoxide (DMSO). TTX citrate was diluted in ddH_2O. All chemicals were stored at −20 °C, and on the day of the experiment, pharmacological agents were thawed and diluted in aCSF to reach their final concentration. The final bath solutions did not exceed 0.1% DMSO or 0.002% EtOH.

Antibodies

The anti-aromatase primary antibody (rabbit, polyclonal; 1/2000; generously provided by Dr Colin Saldanha) has been extensively used and its specificity has been validated in zebra finch tissue using western blots (Saldanha et al. 2000); it is a good marker for NCM (Ikeda et al. 2017). Neurobiotin tracer (SP-1120; Vector Laboratories) was dissolved at 3 mM in internal solution, and DyLight 488 streptavidin (1/200; SA-5488; Vector Laboratories) was used as a fluorescent secondary antibody against biotin. Anti-rabbit conjugated with Alexa 594 (1/200 or 1/500; A11012; Invitrogen) was raised in goat. There were multiple concentrations used for the same secondary antibodies, because titrations were performed in the middle of this project which demonstrated comparable staining using substantially less product. Our goal in performing histology was to determine if specific, pre-recorded neurons expressed aromatase, and we did not quantify expression patterns across sections.

Viral surgery

Viral methods followed those validated in a separate study showing the restricted expression of AAV9-GAD1 to inhibitory neurons (Spool et al. 2021). Subjects were anesthetized using isoflurane (2% during induction; 1.5% during surgery; 0.8–1.0 L O_2/min) or by intramuscular injection of 30–45 μL Equithesin (based on weight). Each subject was mounted to a stereotaxic frame, the angle of the head set to 45°, the scalp exposed, and 20 μL of 2% lidocaine (in 100% EtOH) injected subcutaneously. The scalp was then incised above the midline bifurcation, and bilateral craniotomies were performed above the nidopallium (0.9 mm rostral, 0.7 mm lateral to the bifurcation of the mid-sagittal sinus), through which the virus-containing glass pipette of a programmable nanoliter injector (Nanoject iii; Drummond Scientific) was lowered 1.4 mm into the NCM. Adeno-associated virus (AAV) vectors encoding GAD1-Cre (pAAV-hGAD1-FLAG-NLS-Cre; 1.25 × 10^12 vg per mL; made in-house) and a Cre-dependent GCaMP6f (AAV9-CAG-Flex-GCaMP6f-WPRE-SV40; UPenn Vector Core, 2.62 × 10^12 vg per mL) were co-injected into this region at a rate of 1 nL/s (5 cycles of 125 nL; 60 s latency between cycles; 10 min latency between final injection and injector retraction). Once the pipette was fully retracted and checked for blockage, the craniotomies were filled with a low toxicity silicone adhesive (Kwik-Sil; World Precision Instruments), and the scalp was sealed with cyanoacrylate. Imaging experiments took place 3–6 weeks after viral injections to ensure sufficient expression.

Sample preparation

Each subject was rapidly decapitated, the brain was then extracted onto a chilled petri dish, and the lateral portions were carefully dissected away with a razor blade (i.e. a sagittal cut in each hemisphere ~3 to 3.5 mm from midline) and disposed. For the calcium imaging experiments, the skull was removed and submerged in ice cold cutting solution for 20 min before vibratome sectioning. For all experiments, the left and right hemispheres were dissociated and mounted on the lateral surface to a specimen disk (14046327404, Leica Biosystems) with cyanoacrylate, and the disk was secured inside the buffer tray of a vibrating microtome (VT1000S, Leica Biosystems) and covered with ice cold, oxygenated cutting solution. Slices 250–300 μm thick containing NCM were collected and immediately transferred to a heated, oxygenated aCSF (35–37 °C). Following 30–60 min under these conditions, slices were stored in oxygenated aCSF at room temperature. Slices were individually transferred to a perfusion chamber, where they were perfused with oxygenated, room temperature aCSF at a rate of 1.25 mL/min during experimentation.

Intracellular electrophysiology

Whole-cell patch clamp recordings were obtained from neurons within the NCM in brain slices from adult male and female zebra finches. Tissue was imaged using a charge-coupled camera (QIClick; QImaging) mounted to a fixed stage microscope equipped with DIC and fluorescence optics (Eclipse FN1; Nikon) and a water immersion objective (CFI Fluor; 40×; NA = 0.8; WD = 2.0 mm; Nikon). Glass pipettes were pulled from borosilicate glass capillary tubes (1B150F-4; World Precision Instruments) using a 2-stage, vertical puller (PC-10; Narishige International USA). Pipettes had a tip resistance of 4–8 MΩ when backfilled with internal solution, which was generally coupled with neurobiotin tracer (Vector Laboratories) for identification post-recording. Positive pressure (∼2.2 psi) was applied to each pipette while moving through aCSF and tissue until a target cell was located. Following the achievement of a giga-ohm seal, the membrane was ruptured by applying negative pressure (∼−1 psi) accompanied by short voltage pulses (300–1,024 mV; 0.3–1.0 ms) when necessary. Once a whole-cell configuration was successfully achieved, series resistance and slow capacitive transients were compensated. Each recording configuration was allowed to stabilize for a minimum of 5 min before any protocols were executed (Dagostin et al. 2015). Current or voltage signals were Bessel filtered at 2 kHz, digitized, and acquired at 10–40 kHz using a HEKA amplifier (EPC 10 USB; HEKA Elektronik) driven by PATCHMASTER software (v2x73.2; HEKA Elektronik).

Voltage clamp

Voltage clamp was used to investigate how E2 modulates network inputs to NCM neurons. For experiments isolating miniature inhibitory post-synaptic currents (mIPSCs), a CsCl-based internal solution was used to block potassium channels. Once a stable whole-cell configuration was established, the holding potential was set to −80 mV. mIPSCs were collected in the presence of TTX citrate (1 μM), a potent sodium channel inhibitor, and DNQX (20 μM), an AMPA and kainate receptor antagonist, while mEPSCs were collected in the presence of TTX citrate (1 μM) and bicuculline (20 μM), a GABA-A receptor antagonist. After 10 min under baseline conditions, E2 (50 or 100 nM) was introduced to the aCSF, and recordings proceeded for an additional 10 min. The bath-applied doses of E2 used in this study were chosen to match the magnitude of doses shown efficacious in prior slice electrophysiology studies (1–100 nM; Huang and Woolley 2012; Kow et al. 2006; Moenter and Chu 2012). In a subset of mIPSC recordings, bicuculline (20 μM) was added to the aCSF for a final 10 min to confirm that the recorded inward currents were GABA-A dependent. Rundown experiments of equivalent duration were performed in a separate set of cells, in which either mIPSCs or mEPSCs were recorded in the presence of synaptic blockers, but no additional pharmacological agents were added. Data were acquired at 10 kHz in PATCHMASTER and analyzed using Igor Pro, where they were smoothed using a box algorithm with a 10-point sliding average. Miniature events were detected with a custom script that used waveform-based template matching based on a sliding template technique (Clements and Bekkers 1997). Miniature events were evaluated for each recording and validated by multiple observers following detection using the template matching algorithm.

Current clamp

To examine the effects of E2 on the intrinsic excitability of individual NCM neurons, we utilized current clamp with a potassium gluconate internal solution. Protocols alternated between recording spontaneous voltage at rest and voltage deflections following current injections. Stimulations consisted of step hyperpolarizing and depolarizing current injections (500–2000 ms) at intervals of 10 or 20 pA relative to baseline holding current. E2 was administered following 10 min of baseline recording. Rundown experiments of equivalent duration were performed in a separate set of cells, in which slices were maintained in external solution but no additional pharmacological agents were added. Series resistance, slow capacitive transients, holding current, and RMP were measured at ∼5-min intervals across all experiments to monitor the quality of the recording access to the cell. All data were acquired in PATCHMASTER at 40 kHz, then analyzed using Igor Pro (WaveMetrics), and processed using a 1 kHz low-pass filter. Steady-state voltage (SSV), AP repolarization time constant (τ_{apr}), RMP, and half-width were each calculated using a custom script written in Igor Pro. When a neuron is naturally or artificially hyperpolarized, inward-rectifying cation channels can be activated, wherein the membrane voltage displays a brief depolarization, or "sag," before reaching SSV. Sag index, rheobase, AP latency, and latency jitter were each quantified from the experimental traces. Sag index was defined as the most negative voltage deflection of the largest hyperpolarizing current pulse minus the SSV of that sweep, divided by the SSV, as has been previously described (Farries et al. 2005; Dorris et al. 2015). Rheobase was defined as the minimum positive current injection to elicit at least one AP. AP latency was defined as the time required to reach threshold potential following the onset of a depolarizing current pulse, and jitter was defined as the trial-by-trial precision of this measure. Both the latency and jitter were derived from the second depolarizing current injection to elicit an AP (i.e. one current sweep above rheobase). Peak firing was defined as the maximum number of APs elicited per set of current injections. Input resistance (IR) was estimated via linear regression from the SSV of the first 5 hyperpolarizing injections. We also calculated IR by calculating the SSV of only the 3 smallest hyperpolarizing current injections, to determine whether our first measurement of IR was sensitive to the activation of voltage-gated rectifier channels beyond this range, and the results reported below were not different in this non-rectified range. The τ_{apr} was calculated by fitting an exponential function to the falling

phase of the first AP elicited from a current injection at rheobase. Representative waveforms were obtained from spontaneously occurring APs (Fig. 2H).

To examine the effects of E2 on the intrinsic plasticity of APs (Daou and Margoliash 2020), we also collected a set of features from the first AP at rheobase using custom Python scripts. These included the AP threshold (mV), AP peak (mV), the duration of the afterhyperpolarization (ms), the depth of the afterhyperpolarization (mV), and the afterhyperpolarization half-duration (ms). Features were collected at baseline and at 4 time points (up to 20 min) following E2 treatment.

Ex vivo calcium imaging

All slices were visualized in low-light conditions at the Nikon Center of Excellence Light Microscopy Core in the University of Massachusetts Amherst, using a multiphoton, confocal microscope (A1R; Nikon). GAD1-GCaMP6f fluorescence was excited at 900 nm with a tunable laser (Ti: Sapphire; Spectra Physics). To evaluate the viability of GCaMP6f imaging in our preparation, we performed resonant line-scan imaging (512 × 1 pixels) using a water immersion objective (40×; NA = 1.15; RI = 1.33; Apo 40× WI λS DIC N2; Nikon) to isolate single, AP-like calcium transients at high temporal resolution. Data were collected at a rate of 15.8 kHz to detect spontaneous, fast calcium transients and were smoothed with a Hamming convolution (Python Pandas library; representative transients shown in Fig. 5D). For recordings in which the field of view was not restricted (512 × 512 pixels) when we bath applied E2, data were collected utilizing galvano scanning at a rate of 0.24 Hz with a water immersion objective (25×; NA = 1.10; RI = 1.33; Apo LWD 25× 1.10 W DIC N2; Nikon).

All full-field recordings were corrected for X-Y movement using alignment features in NIS-Elements Advanced Research (Nikon), which aligns prominent fluorescent structures from each frame with their X-Y position in the first frame. Each recording was segmented based on changes to the external solution (pre-treatment, treatment, washout) in order to increase the effectiveness of X-Y motion correction. Segments containing treatment or washout were each normalized to an average of the last 120 s of the previous segment (e.g. a segment containing E2 treatment would be normalized to an average of the final 120 s of pre-treatment). Pre-treatment (baseline) segments were normalized to an average of the first 120 s of the recording. If substantial movement in the Z plane was observed at the end of a recording, we removed this segment from our analysis. If movement in the Z plane was pervasive throughout, however, we omitted the full recording.

Regions of interest (ROIs) were defined on a maximum intensity projection in NIS-Elements Advanced Research by manual intensity thresholding, incorporating smoothing (×1), cleaning (×2), and a diametric filter (6–100 μm) in order to reduce the number of small ROIs which would be more susceptible to errors in X-Y alignment. ROIs at the edge of the frame were omitted, since slight X-Y movement could push these out of the field of view. Changes in fluorescence were calculated using the formula $\Delta F/F_0$, and data were then averaged across 34 s bins. Units were not considered responsive to treatment unless their fluorescent signal changed by at least 10% for 3 out of any 4 consecutive bins during the treatment period.

Immunohistochemistry

During current-clamp experiments, we routinely included neurobiotin in our internal solution for the purpose of identifying neurons post-recording. After recording, tissue sections were drop-fixed in 4% PFA for a minimum of 12 h before being transferred to a cryoprotective solution and stored at −20 °C. Immunohistochemistry (IHC) was performed in order to locate recorded neurons and identify whether or not they expressed aromatase. To begin, sections were washed in 0.1 M PB for 1.5 h (6 washes of 15 min). We then permeabilized and blocked the tissue by incubating each section for 2 h in a solution of 10% normal goat serum (NGS) and 90% PB containing 0.3% Triton X (0.3% PBT). Primary anti-aromatase (1/2000) was diluted with 10% NGS in 0.3% PBT, and sections were incubated in this solution at room temperature for 1 h before being stored at 4 °C for 2 consecutive nights (∼40 h). Following primary antibody incubation, sections were washed in 0.1% PBT for 45 min (3 washes of 15 min). Secondary antibodies (anti-rabbit Alexa 594, and DyLight 488 streptavidin) were diluted in 0.3% PBT, and the tissue sat in this solution for 1 h at room temperature. Finally, the sections were washed for 30 min in 0.1% PBT (3 washes of 10 min) and mounted to gelatin-coated slides using ProLong Diamond Antifade Mounting Medium (Thermo Fisher). For incubations and washes, tissue was placed on an orbital plate shaker at a speed of 90 RPM. Histologically processed tissue was visualized at the University of Massachusetts Amherst's Nikon Center of Excellence using a confocal microscope (NA1; Nikon). Laser power and gain were manually established for each section based on strength of the fluorescence.

Extracellular electrophysiology

In vivo recording data were analyzed from a previously published data set (Remage-Healey et al. 2010). In that study, 100uM fadrozole (FAD; potent aromatase inhibitor) retrodialyzed into the NCM caused a rapid suppression of burst firing of single neurons. Based on our current findings that uncover the role of estrogens in shaping temporal precision of NCM neurons in ex vivo slice recordings, we examined whether FAD caused a disruption of trial-by-trial correlation in auditory-evoked activity of NCM neurons in that same set of spike trains (12 cells from 5 birds). Spike trains were evaluated for the trial-by-trial correlation in spike timing in response to conspecific song playback across 20 trials. A custom Python algorithm compared responses to stimuli using the Rcorr

metric (Schreiber et al. 2003) after smoothing spike trains with a Gaussian filter (16-ms standard deviation). Rcorr values were averaged for each neuron across stimuli and these values were compared across treatment groups (aCSF vs. FAD).

Statistics

Statistical analysis and visualization were performed in Python using numpy, pandas, neo, seaborn, elephant, matplotlib, and other libraries (Hunter 2007; Pedregosa et al. 2011; Garcia et al. 2014; Yegenoglu et al. 2018; Harris et al. 2020; Waskom 2020) and OriginPro. One-way and 2-way analysis of variance (ANOVA) and Student's *t*-tests were used, with Greenhouse–Geisser and Bonferroni corrections when necessary.

Results

Confirmation of NCM phenotypes by intrinsic membrane properties

Neurons in the caudal pallium of songbirds exhibit intrinsic properties that can be broadly classified into tonic versus phasic firing states. Tonically responsive neurons (i.e. those without strong accommodation to current depolarizations) generally display higher IR than those with transient or phasic profiles (Dagostin et al. 2015; Chen and Meliza 2018). To establish classification phenotypes in NCM neurons, we conducted whole-cell current-clamp recordings and examined a range of active and passive membrane properties. We were guided in our cell classifications by a prior comprehensive study using similar methods in the same brain region (Dagostin et al. 2015). We observed similarly distinct subtypes characterized by voltage responses to current injections (Fig. 1A). To begin, we combined cells with "transient" and "phasic" adaptation profiles based on their degree of spiking accommodation (T/P; strong accommodation) as distinct from "tonic" profiles (little to no accommodation), and membrane properties were largely consistent with those previously reported (Dagostin et al. 2015). In our population, no differences were observed between tonic versus T/P neurons in terms of resting membrane potential (RMP; -65.2 ± 2.0 vs. -67.0 ± 2.8 mV, $P = 0.59$, Student's unpaired 2-tailed *t*-test; Fig. 1B), AP peak (38.1 ± 2.7 vs. 32.2 ± 3.2 mV, $P = 0.18$, Student's unpaired 2-tailed *t*-test; Fig. 1C), AP half-width (2.15 ± 0.72 vs. 3.46 ± 0.96 ms; $P = 0.16$, Student's unpaired 2-tailed *t*-test, Fig. 1D), and AP repolarization tau (1.84 ± 0.66 vs. 2.11 ± 0.43 ms; $P = 0.24$, Student's unpaired 2-tailed *t*-test, Fig. 1E). However, in agreement with prior findings, tonic neurons had significantly lower rheobase (current threshold) than T/P (22.3 ± 3.4 vs. 66.0 ± 18.4 pA, $P = 0.04$, Student's unpaired 2-tailed *t*-test; Fig. 1F) and significantly higher IR (630.8 ± 109.7 vs. 283.8 ± 30.7 MΩ, $P < 0.01$, Student's unpaired 2-tailed *t*-test; Fig. 1G). Together, these results replicated prior findings in NCM and provided a foundation to use these methods in NCM slice recordings for subsequent tests of estrogen-dependent modulation.

Estradiol rapidly increases membrane conductance in a population of physiologically distinct NCM neurons

To examine how 17-beta-estradiol (E2) regulates the electrophysiological properties of NCM neurons, we exposed sagittal slices containing NCM to E2 (50 nM) under current-clamp conditions (Figs. 2 and 3). The active membrane properties used previously to classify NCM neuronal phenotypes can be somewhat variable over longer recording times (e.g. Fig. 3A; see similar switches in firing accommodation state between "tonic" vs. "phasic"; Dagostin et al. 2015). This led us to consider an alternative way to phenotype NCM neurons. We evaluated the distribution of IR at baseline (i.e. pre-E2) and found it was segregated by kmeans one-dimensional clustering (Python via Scikit-learn library; Pedregosa et al. 2011). We therefore classified our recorded population of cells as either low-IR or high-IR neurons (Fig. 2C). The 2 populations of low- versus high-IR neurons differed substantially in their electrophysiological responses to E2. Specifically, high-IR neurons were unresponsive to E2 ($F_{1.48, 2.96} = 0.36$, $P = 0.435$, one-way repeated measures ANOVA, Greenhouse–Geisser correction). By contrast, neurons with initially low-IR significantly increased membrane conductance (i.e. further IR reduction among all recorded low-IR neurons) on a rapid timescale within ~10 min ($F_{3, 21} = 10.08$, $P = 0.0002$; Bonferroni post hocs: low IR, pre vs. 10 min E2, $P = 0.0051$, low IR, pre vs. 16 min E2, $P = 0.00017$; low IR, pre vs. 20 min washout, $P = 0.032$) (Fig. 2A and B). Therefore, the initial passive membrane properties of NCM neurons (low-IR vs. high-IR at baseline) were highly predictive of their intrinsic property profile in response to the acute actions of E2.

The passive membrane IR reflects underlying channel populations and conformations (i.e. ion permeabilities) and is typically in register with a number of other membrane properties (Oertel 1999). To gain insight regarding correlated and orthogonal features of these high- versus low-IR neuronal phenotypes, we further investigated their passive and active membrane properties. Neurons in the songbird striatum with a sag index ≥ 0.1 typically display inward rectification with considerable time dependency (Farries et al. 2005). In NCM, neither population contained neurons with a sag index exceeding 0.1, nor were there significant differences between low-IR and high-IR neurons in sag index (0.022 ± 0.004 vs. 0.028 ± 0.009, $P = 0.52$, Student's unpaired 2-tailed *t*-test; Fig. 2D). Furthermore, neither population showed an effect of E2 on this measure (low IR: pre-treatment 0.019 ± 0.003; following E2 0.024 ± 0.004, $P = 0.39$; high IR: pretreatment 0.031 ± 0.006; following E2 0.037 ± 0.004, $P = 0.50$). There were also no significant differences between low IR and high IR neurons in terms of RMP (-67.7 ± 2.8 vs. -61.1 ± 3.2 mV, $P = 0.16$, Student's unpaired 2-tailed *t*-test; Fig. 2E). By contrast, the half-width of APs elicited from current stimulation differed between the 2 cell phenotypes. Low-IR neurons had longer AP durations than those with high-IR (3.0 ± 0.3

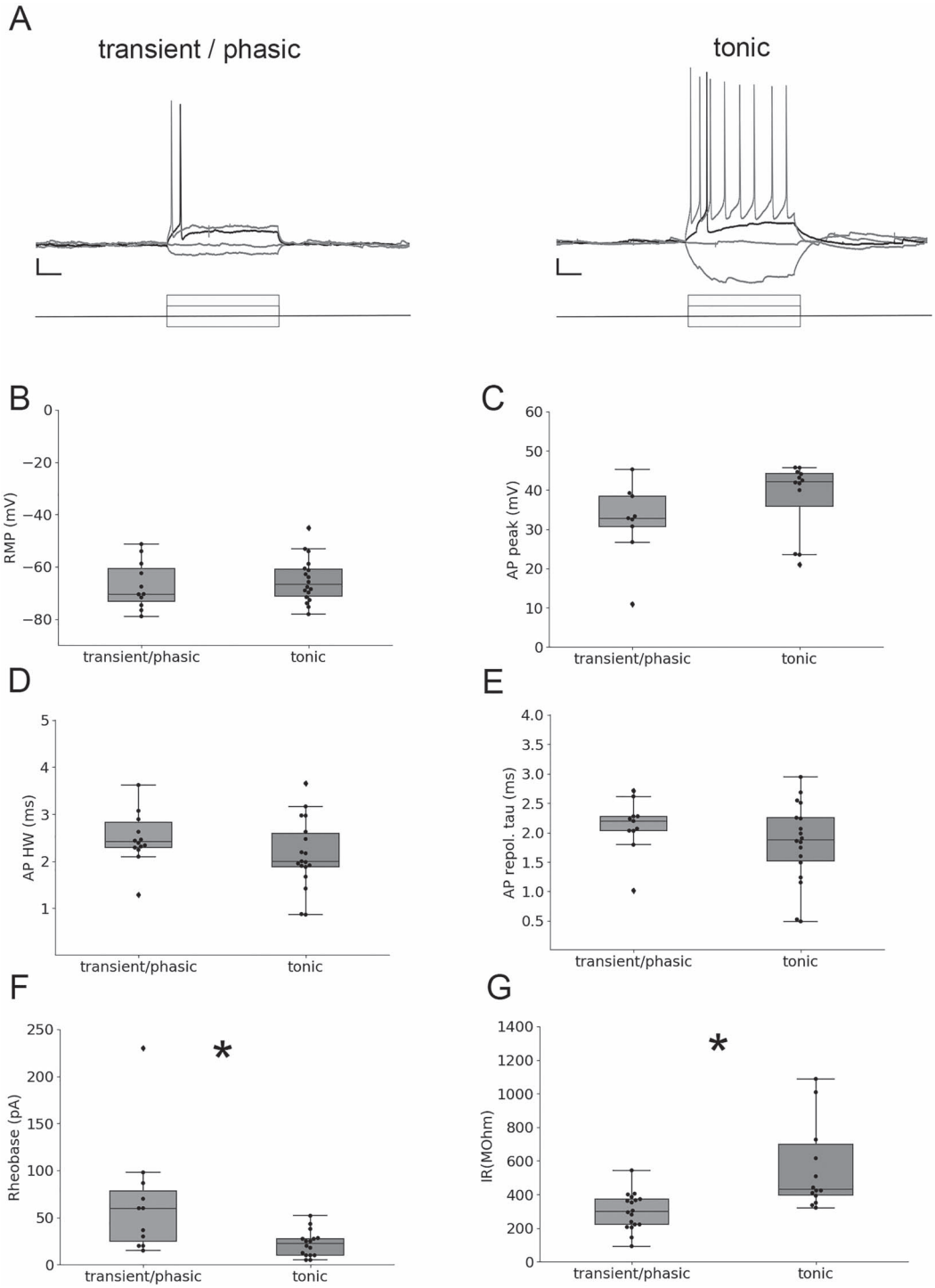

Fig. 1. Electrical phenotype classifications during current-clamp recordings segregate NCM neurons by rheobase and IR. A) Representative voltage traces illustrating classification differences between transient/phasic neurons versus tonic neurons in NCM. Rheobase is plotted in black, all other voltage traces plotted in gray; only a subset of voltage traces and current-step injections are plotted for clarity. Plotted current steps are 50 pA. Scale bar = 10 mV; 100 ms. Resting membrane potential (B, RMP), AP peak (C), AP half-width (D, AP HW), and AP repolarization tau (E) were not different between tonic ($N = 19$ cells) versus transient/phasic ($N = 11$ cells) cell type categories in response to current stimulation. By contrast, rheobase (F) and IR (G) were each significantly different between the 2 classification schemes. $^*P < 0.05$.

vs. 1.7 ± 0.2 ms, $P = 0.01$, Student's unpaired 2-tailed *t*-test; Fig. 2F), and this was consistent with the waveform profile of spontaneously occurring spikes we recorded (Fig. 2C). Relatedly, there was a significant difference in the time constant of the AP repolarization phase (low-IR: 2.7 ± 0.4 vs. high-IR: 1.3 ± 0.2, $P = 0.01$; Fig. 2G), suggesting a cell-type difference in cation efflux, and consistent also with observed faster kinetics for the depolarization phase among high-IR neurons (Fig. 2C). Taken together, these data indicate that low-IR neurons exhibit several passive and active properties that differ from those with high-IR, the most prominent of which is the sensitivity of

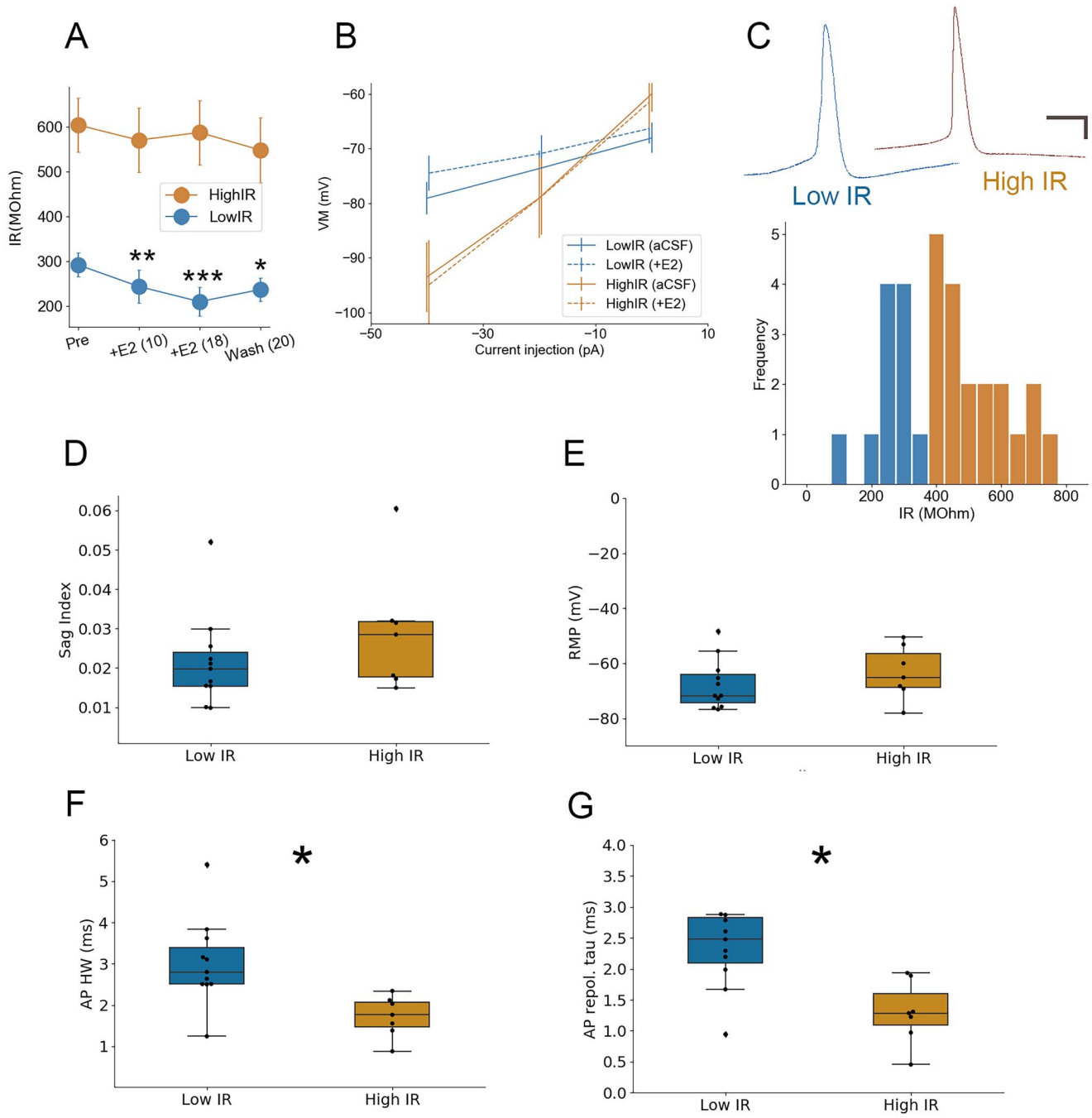

Fig. 2. Only NCM neurons with low IR respond to bath-applied 17-beta-estradiol (E2). A, B) Differential change in passive membrane conductance (IR) among high-IR ($N = 8$) versus low-IR ($N = 11$) neurons in NCM in response to bath application of 50 nM E2. In panel A, numbers in parentheses denote time in minutes following E2 application. C) Top: Representative waveforms during recordings of spontaneous activity in low-IR versus high-IR neurons. Scale bars = 10 mV, 10 ms. Bottom: Histogram of IR from the population of recorded cells, with a cluster split at 400 MOhm (colors denote one-dimensional k-means algorithm via Scikit-learn Python library; (Pedregosa et al. 2011). D) Properties of high- versus low-IR NCM neurons in terms of sag index (D), resting membrane potential (E), AP half-width (F), and AP repolarization tau (G). *$P < 0.05$.

low-IR neurons, but not high-IR neurons, to bath applied 50 nM E2.

Estradiol modulates excitability and enhances AP timing precision in neurons with low IR

The observation that E2 rapidly increased membrane conductance among low-IR neurons (Fig. 2A and B) predicts concomitant effects on evoked spike latency and precision (Oertel 1999; Dagostin et al. 2015; Franzen et al. 2015). Consistent with this prediction, we found that low-IR neurons responded to E2 with a reduction of the peak firing rate (Fig. 3A and B) while high-IR neurons did not ($F_{2.28, 38.76} = 11.75$, $P < 0.001$, 2-way repeated measures ANOVA for effects of treatment; $F_{2.28, 38.76} = 6.56$, $P < 0.001$, 2-way repeated measures ANOVA for treatment-by-cell-type interaction; high-IR, $F_{1.88, 13.2} = 0.90$, $P = 0.42$, one-way repeated measures ANOVA for effects of treatment; low-IR, $F_{2.24, 22.44} = 15.31$,

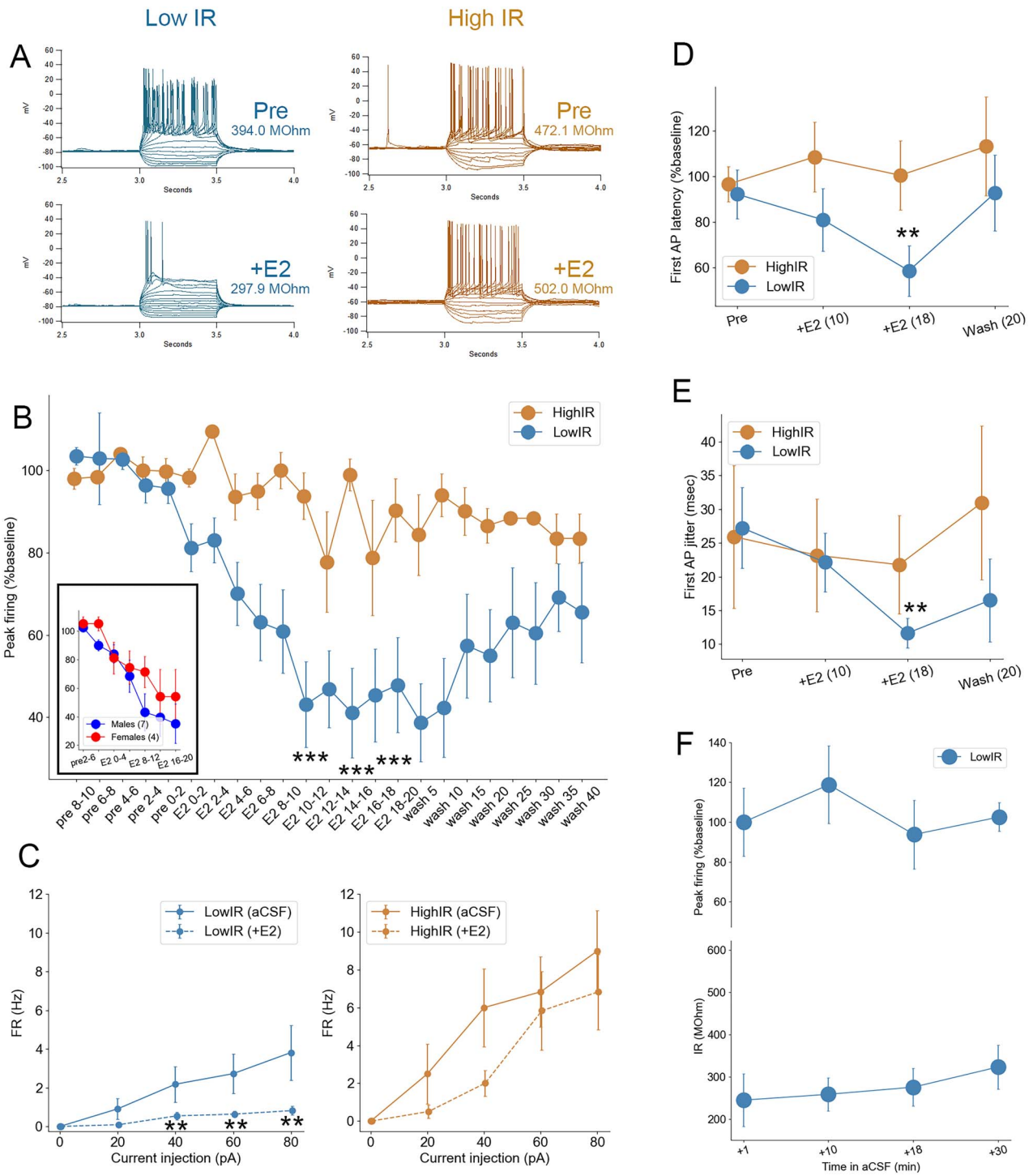

Fig. 3. Estradiol (E2) rapidly changes intrinsic excitability and temporal precision in NCM neurons with low IR. A) Representative current-clamp traces for a low-IR (left) versus high-IR (right) neurons in NCM. Note the changes in active and passive membrane properties in response to 50 nM E2 in low-IR neurons exclusively, including spiking activity (peak firing) as well as IR (inset numbers) for each cell. B) The peak firing (maximum number of spikes evoked per series of current steps; expressed as a % change from the 10 min baseline period) of low-IR neurons ($N = 11$) drops significantly 8–10 min following bath application of 50 nM E2, while peak firing is not significantly altered in high-IR neurons ($N = 8$). Numbers on x-axis denote time in minutes relative to E2 application. Inset: Similar magnitude decrease in peak firing of low-IR neurons observed in males and females. C) *F/I* relationships during baseline (aCSF) and following 8–10 min of 50 nM E2 (+E2) for low-IR (left) versus high-IR (right) neurons. The firing rate (FR) of low-IR neurons was suppressed by 50 nM E2 at all depolarizing current steps from 40 to 80 pA, while no changes on FR were observed in high-IR neurons. D, E) The temporal precision of the first AP evoked at rheobase in low-IR neurons was also enhanced by 50 nm E2, reflected in a quickening of first-AP latency (D) and reduction in first-AP latency jitter (E) in low- but not high-IR neurons. Numbers in parentheses denote time in minutes following E2 application. F) Rundown control experiments in low-IR neurons showing no change in either IR (top) or peak firing (bottom). $^{***}P < 0.001$, $^{**}P < 0.005$.

$P < 0.001$, one-way repeated measures ANOVA for effects of treatment). Accordingly, the relationship between injected current amplitude and AP frequency was also rapidly regulated by E2 in low-IR but not high-IR neurons (Fig. 3C). In a separate analysis, we examined whether the drop in peak firing in low-IR neurons was dependent on sex. While the effect of E2-treatment was still evident in this analysis ($F_{2.09, 25.09} = 4.97$, $P = 0.01$, one-way repeated measures ANOVA for effects of treatment), there was no detectable difference between cells from males versus females ($F_{2.09, 25.09} = 0.57$, $P = 0.58$, one-way repeated measures ANOVA for treatment*sex interaction, Fig. 3B inset). Therefore, low IR neurons in NCM from both males and females exhibit an E2-dependent, rapid reduction in peak firing.

Furthermore, exposure to E2 rapidly, significantly, selectively, and reversibly reduced AP latency (i.e. time to first evoked AP from onset of depolarizing current injection) among low-IR, but not high-IR, neurons ($F_{3.04, 45.68} = 1.60$, $P = 0.20$, 2-way repeated measures ANOVA for effects of treatment; $F_{3.05, 45.68} = 3.64$, $P = 0.019$, 2-way repeated measures ANOVA for treatment-by-group interaction; low-IR, $F_{5, 50} = 3.31$, $P = 0.012$, one-way repeated measures ANOVA for effects of treatment; low-IR, pre vs. 12–16 min E2, $P = 0.005$, Bonferroni; Fig. 3D). In addition, AP onset precision increased following E2 treatment among low-IR neurons (27.2 ± 6.0 to 11.6 ± 2.2, $P = 0.009$, Student's paired, 2-tailed t-test), but not high-IR neurons (25.9 ± 10.6 to 21.8 ± 6.3, $P = 0.55$, Student's paired 2-tailed t-test; Fig. 3E). Importantly, a separate population of low-IR cells exposed to "rundown" conditions (i.e. maintained in external aCSF solution for equivalent duration as in the E2 experiments) showed no significant effects of aCSF bath duration on either IR or peak firing (all $P > 0.05$; Fig. 3F). Together, these findings indicate that E2 rapidly shapes the temporal precision of firing in a select population of NCM neurons, predicted by their low baseline IR.

Estradiol does not influence the intrinsic plasticity of NCM APs

In both populations of low-IR and high-IR neurons, E2 caused no discernable change in the active action potential parameters measured, including peak, threshold, and afterhyperpolarization (Table 1). Therefore, despite an influence on membrane excitability and temporal onset properties in low-IR neurons, E2 did not influence the active currents that contribute to the dynamics of the AP in NCM neurons.

Estradiol response profiles are not predicted by somatic aromatase expression

E2 is synthesized in the brain by the enzyme aromatase, which is abundantly expressed in neurons in a variety of species (see Introduction), including auditory pathways of humans and songbirds. Since low- versus high-IR neurons exhibited a clear divergence in their response profile to bath-applied estradiol, we were curious as to whether they were themselves aromatase-positive. If low-IR neurons are also aromatase-positive, this would be consistent with an acute "autocrine" feedback of local neuroestrogen synthesis (Remage-Healey et al. 2011; Saldanha et al. 2011) on their own intrinsic excitability. We therefore examined whether our recorded NCM neurons also expressed aromatase by including the tracing molecule neurobiotin in the internal recording solution for a subset of our current-clamp recordings. Following the experiment, we histologically processed each section for neurobiotin alongside aromatase expression. Surprisingly, for all neurons histologically recovered after recording, we found no clear segregation of aromatase expression among low-IR (4 aromatase+, 3 aromatase−; e.g. Fig. 4A) or high-IR (2 aromatase+, 1 aromatase−; e.g. Fig. 4B) neurons in NCM (representative cells in Fig. 4). Therefore, while aromatase is a defining marker for the NCM region, it did not clearly distinguish the population of NCM neurons that were unresponsive versus responsive to the rapid actions of E2.

Estradiol regulates inhibitory neurotransmission, but not excitation

The suppression of intrinsic excitability by E2 in NCM could be balanced, offset, or accentuated by acute effects at the level of neurotransmitter release probability. To investigate these possibilities, we recorded miniature postsynaptic currents using whole-cell voltage clamp methods prior to and following exposure to E2 in vitro. We observed a rapid decrease in mIPSC frequency among neurons treated with 50 nM E2 ($F_{4, 48} = 4.37$, $P = 0.0046$, one-way repeated measures ANOVA for effects of treatment; 0–2 min vs. 8–10 min, $P = 0.0053$, Bonferroni; Fig. 5A). This was evident in both males and females, as there was no effect of sex on this outcome ($F_{1, 11} = 1.62$, $P = 0.229$, one-way repeated measures ANOVA for effects of sex, $n = 7$ males, 7 females) and no treatment-by-sex interaction ($F_{4, 44} = 1.287$, $P = 0.289$, one-way repeated measures ANOVA for treatment-by-sex interaction, $n = 7$ males, 7 females). This E2-dependent decrease in mIPSC frequency was also evident in non-normalized data (mean ± sem: baseline: 0.90 ± 0.16; 0–2 min 0.87 ± 0.16; 2–4 min 0.81 ± 0.15; 4–6 min 0.83 ± 0.15; 6–8 min 0.72 ± 0.14; 8–10 min 0.66 ± 0.14). We observed a similar rapid reduction in mIPSC frequency following a higher-dose 100 nM E2 treatment (-1.5 ± 6.5 vs. $-37.7 \pm 7.5\%$, $P = 0.007$, Student's paired 2-tailed t-test), and no change among rundown controls (aCSF alone; -7.2 ± 17.6 vs. $2.5 \pm 14.8\%$, $P = 0.668$, Student's paired 2-tailed t-test; Fig. 5B). There was no effect of E2 at either dose on the amplitude of mIPSCs (all $P < 0.57$), consistent with a specific effect of E2 on inhibitory pre-synaptic release probability onto NCM neurons. In separate experiments examining excitatory synaptic inputs, there was no change in mEPSC frequency for the same dose of 50 nM E2 (one-way repeated measures ANOVA for effects of treatment $F_{4, 44} = 1.15$, $P = 0.34$; Fig. 5C). There was also no change in mEPSC frequency for a separate set of cells

Table 1. AP parameters from NCM neurons of both classes of IR reveal no systematic effects of estradiol (E2) on intrinsic AP parameters for either cell type (all $F < 1.75$, $P > 0.17$).

AP parameter/cell type	Pre	+E2 (5 min)	+E2 (10 min)	+E2 (15 min)	+E2 (20 min)
AHP (ms) High-IR	168.73 + −4.48	170.78 + −3.05	170.72 + −4.53	168.66 + −5.29	172.91 + −6.28
AHP (ms) Low-IR	171.14 + −4.99	171.09 + −5.36	167.93 + −3.32	166.66 + −2.83	166.48 + −3.25
AHP (mV) High-IR	−59.80 + −1.18	−59.31 + −0.96	−58.24 + −0.77	−57.84 + −0.74	−56.66 + −1.21
AHP (mV) Low-IR	−57.47 + −2.22	−57.02 + −2.03	−55.23 + −2.21	−54.80 + −2.35	−54.05 + −2.56
AHP ½ duration (ms) High-IR	4.96 + −1.21	5.11 + −1.11	5.38 + −1.18	4.53 + −1.10	4.83 + −1.25
AHP ½ duration (ms) Low-IR	6.88 + −0.46	7.06 + −0.55	7.18 + −0.58	6.92 + −0.38	7.69 + −0.61
AP threshold (mV) High-IR	−42.37 + −1.67	−42.23 + −1.68	−41.18 + −1.37	−41.40 + −1.65	−40.11 + −2.40
AP threshold (mV) Low-IR	−45.00 + −2.31	−44.45 + −2.41	−43.75 + −2.29	−43.82 + −2.22	−44.1 + −2.72
AP peak (mV) High-IR	28.98 + −4.24	31.04 + −4.39	36.81 + −3.49	35.40 + −4.25	35.26 + −2.98
AP peak (mV) Low-IR	31.72 + −3.32	36.69 + −3.08	33.47 + −2.52	34.27 + −2.73	33.72 + −2.51

There were also no observed differences between IR cell types at baseline (pre) for any parameter (all $P > 0.21$).

exposed to rundown conditions ($F_{4, 20} = 0.72$, $P = 0.59$; Fig. 5C). The amplitude of mEPSCs did not change during treatment with either E2 or aCSF rundown (all $P < 0.44$; Fig. 5C inset). Together, these findings indicate that E2 rapidly suppresses spontaneous inhibitory neurotransmitter release in NCM but does not directly influence excitatory neurotransmission in NCM.

There is substantial heterogeneity in inhibitory neuron populations in NCM (Ikeda et al. 2017; Pagliaro et al. 2020). The acute effects of E2 on inhibitory synaptic transmission in NCM could be due to a uniform influence of E2 on inhibitory neurons or a combination of heterogeneous actions (i.e. small increases together with larger decreases in inhibitory neurotransmitter release). To explore these possibilities, we performed calcium imaging in which NCM neurons were transduced with an AAV carrying the genetically encoded calcium indicator GCaMP6f. Expression was restricted to inhibitory neurons by using the GAD1 promoter (i.e. "GAD1-GCaMP" neurons; (Spool et al. 2021). In pilot experiments, we used resonant line-scan imaging to verify that individual fast calcium transients in GAD1-GCaMP neurons were detectable in NCM slices (Fig. 5D). In separate experiments with E2 treatments, the field of view was expanded to a 512 × 512 pixel square within the bounds of NCM, and spontaneous fluorescence transients from ROIs in these recordings were quantified before and after exposure to E2. Surprisingly, bath application of 50 nM E2 caused 29% of the inhibitory units we observed to increase their fluorescence by an average of 30.3%, while 20% decreased their signal by an average of 16.1%, and 51% remained stable (i.e. did not exceed a positive or negative change of 10% in 3 out of 4 consecutive bins; Fig. 5D and E). Therefore, E2 caused large increases and decreases in the activity of inhibitory neurons within NCM, reflecting a heterogeneity in estrogen actions embedded in the NCM network.

Estrogenic modulation requires activation of a G protein-coupled estrogen receptor (GPER1)

Estradiol acts primarily on classical receptors ERα and ERβ, as well as at the nonclassical, membrane-bound GPER1 (Vail and Roepke 2019; Cao and Meitzen 2021). The rapid timescale of changes to the membrane properties of NCM neurons following E2 treatment suggests a role for acute, membrane-initiated actions. Prior work has demonstrated that NCM neurons express GPER1 (Acharya and Veney 2012) and are sensitive to GPER1 receptor blockade (using the selective antagonist G36; Krentzel et al. 2018). To test whether the effects of E2 on the intrinsic membrane properties of low-IR NCM neurons are also blocked by G36, we treated low-IR neurons that were recorded in the whole-cell current-clamp configuration with G36 followed by E2. We found that G36 pre-treatment prevented the actions of E2 on passive and active membrane properties. Specifically, G36 blocked the E2-dependent drop in both IR ($F_{1.43, 4.29} = 0.34$, $P = 0.66$, one-way repeated measures ANOVA for effects of treatment comparing G36 with G36 + E2 epochs; Fig. 6A), as well as depolarization-evoked peak firing in low-IR neurons ($F_{6, 12} = 1.41$, $P = 0.29$, one-way repeated measures ANOVA for effects of treatment comparing G36 with G36 + E2 epochs; Fig. 6A). These findings are consistent with a GPER1-dependent mechanism for the rapid actions of E2 on the firing state of low-IR neurons in NCM.

Blocking estrogen production results in a desynchronized neuronal response to birdsong in vivo

Suppressing membrane GPER1 activation not only reduces the stimulus-evoked activity of NCM neurons in vivo, but also their temporal coding, as measured by the accuracy of a pattern classifier (Krentzel et al. 2018). Similarly, suppressing neuroestrogen production in NCM

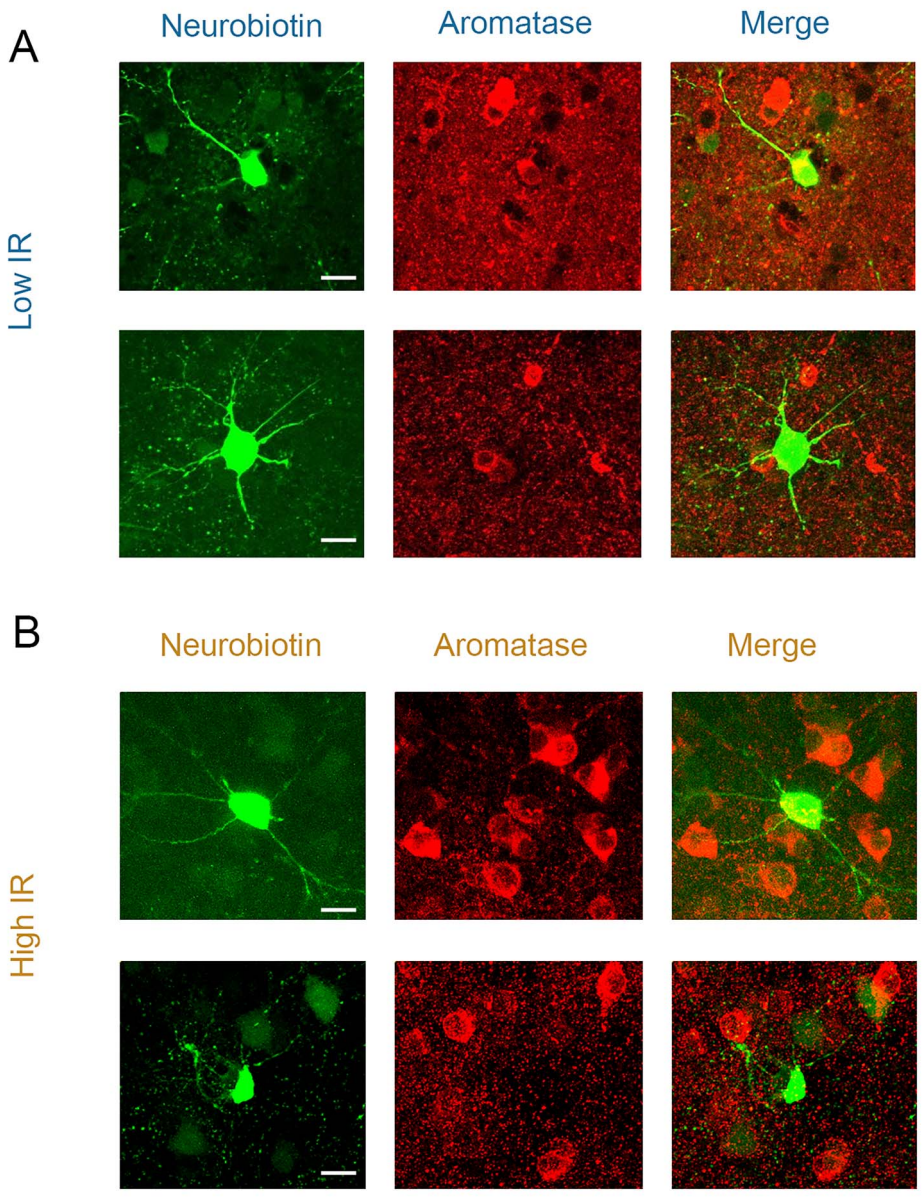

Fig. 4. Aromatase expression is not restricted to high- or low-IR neurons. A) Recorded low-IR neurons which did express aromatase (top) and those which did not (bottom) despite surrounding aromatase positive cells. B) Recorded high-IR neurons which did express aromatase (top) and those which did not (bottom) despite surrounding aromatase positive cells. For each row, green (left; 488 nm) is internal solution neurobiotin filled during current-clamp recordings, while red (middle; 594 nm) is antibody-labeled aromatase (merge at right). Scale bars = 10 μm.

with the aromatase blocker fadrozole (FAD) impairs performance on an auditory-association operant task (Macedo-Lima and Remage-Healey 2020) and dampens the song-evoked firing of NCM neurons (Krentzel et al. 2020). In light of our ex vivo findings presented above, we therefore reasoned that neuroestrogen synthesis in NCM could contribute to the temporal precision of firing patterns of NCM neurons, in vivo. We examined data collected from prior experiments using retrodialyzed fadrozole (FAD; 100 uM), an aromatase inhibitor, during in vivo, extracellular recordings coupled with playback of conspecific birdsong (Remage-Healey et al. 2010). These analyses showed that blocking local neuroestrogen synthesis resulted in a suppression of the trial-by-trial temporal correlation of firing, in 16-ms bin widths, for NCM neurons (Fig. 6B; paired $T = 3.979$; $P < 0.0024$). These findings are consistent with the hypothesis that neuroestrogen synthesis in NCM supports the temporally aligned, highly precise patterns of firing in auditory neurons, a defining feature of this region.

Discussion

This study demonstrates that estrogens rapidly regulate the intrinsic and synaptic properties of sensory neurons to alter their temporal firing precision. We uncovered 2 neuronal populations in the finch auditory pallium that can be distinguished based on 3 orthogonal features: their active membrane properties, IR, and rapid regulation by 17-beta-estradiol (E2). When exposed to E2,

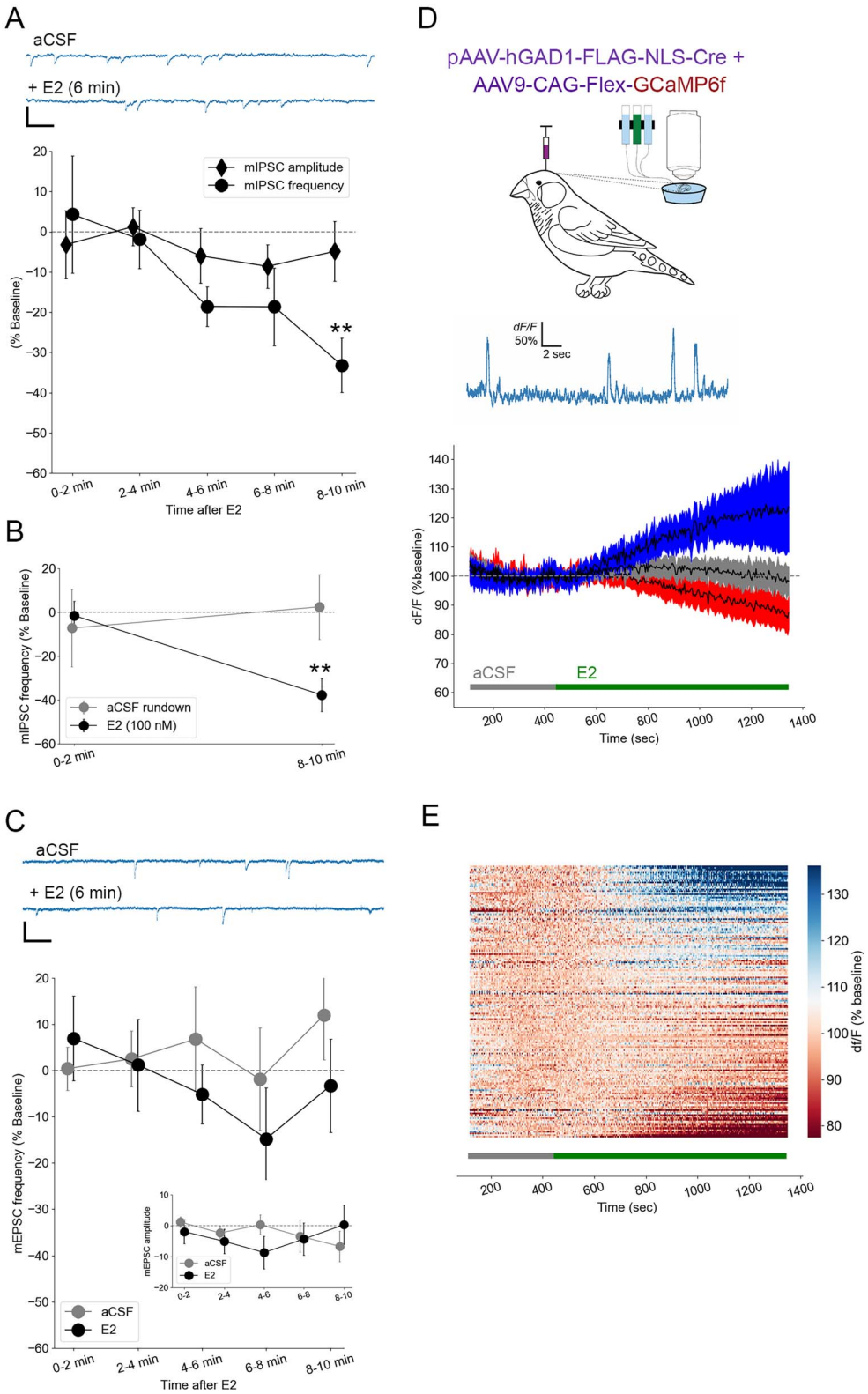

Fig. 5. Estradiol rapidly suppresses miniature inhibitory postsynaptic currents. Bath-applied E2 at 50 nM (A; $N = 13$) and 100 nM (B; $N = 4$) causes a 30%–40% decrease in the frequency of miniature inhibitory postsynaptic currents (mIPSCs) but not their amplitude (A) and no change among rundown controls (B; $N = 6$). $^{**}P < 0.01$ for within-cell differences from baseline. At top of (A) are plotted representative raw current traces of mIPSCs from NCM neurons (scale bar = 20 pA; 25 ms). By contrast, there were no changes in frequency or amplitude (inset) of miniature excitatory post-synaptic currents (mEPSCs) for either aCSF controls ($N = 5$) or 50 nM E2 (C; $N = 13$). At top of (C) are plotted representative raw current traces of mEPSCs from NCM neurons (scale bar = 20 pA; 25 ms). (D) Calcium imaging (% of baseline) reflecting spontaneous cellular and network excitability revealed 3 distinct responses to 50 nM E2 among GAD1-GCaMP6-expressing inhibitory neurons ($n = 288$ ROIs): 29% of units displayed a ~30% increase in activity (blue), 20% demonstrated a ~15% decrease in activity (red), and 51% remained stable (gray). Data were binned at 34 s, and criterion for an increase or decrease in activity was a ±10% change in 3 out of 4 consecutive bins during the treatment period. Top, schematic showing viral injection and ex vivo calcium imaging, and a line-scan imaging session with large, spike-like spontaneous intracellular Ca^{2+} events (D). Same results as shown in (D) are replotted with all ROIs and sorted in a heat map (E).

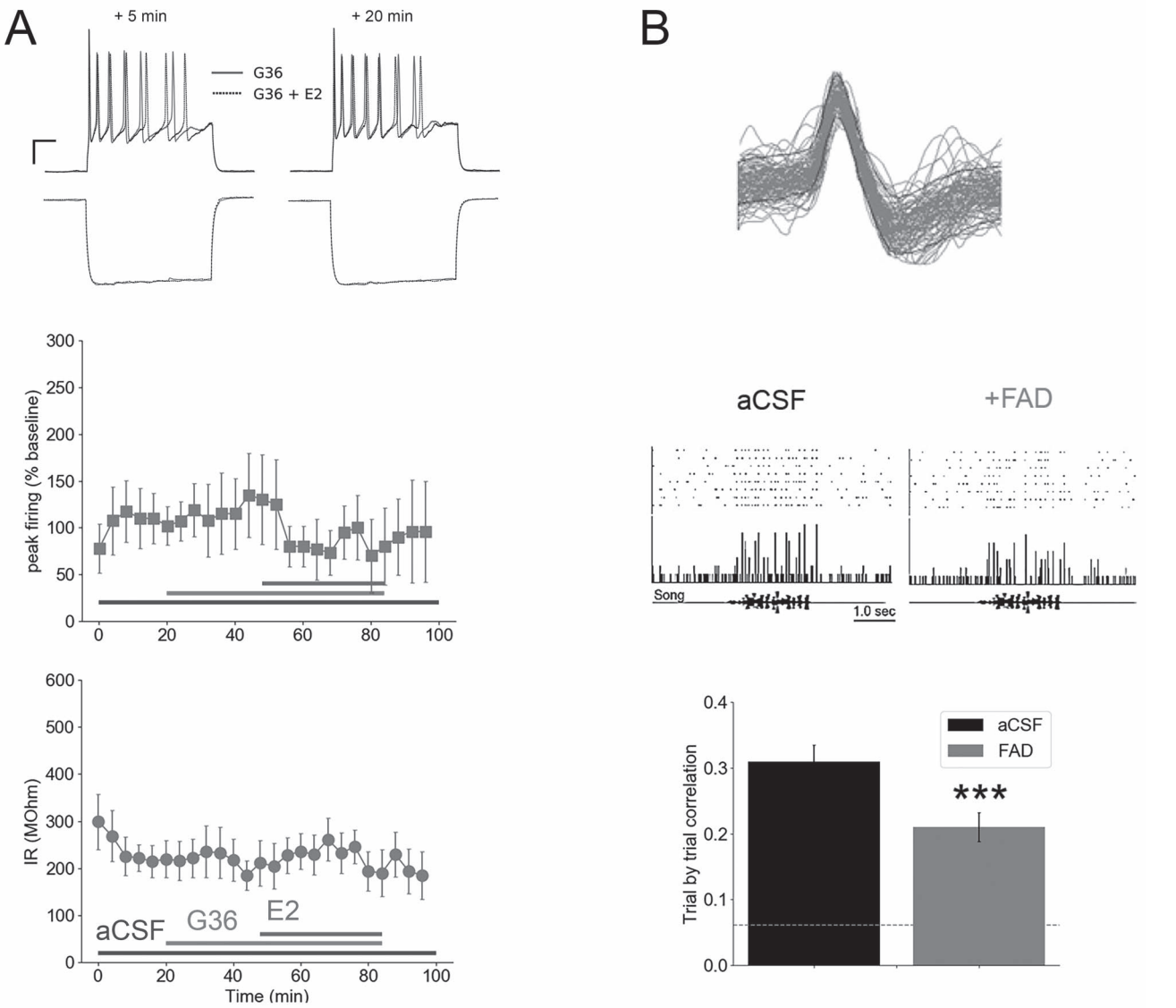

Fig. 6. Rapid estradiol effects require GPER1 activation, and suppressing in vivo brain estrogen synthesis disrupts NCM temporal firing correlations. A) Antagonist experiments with the GPER1 blocker G36 ($N = 5$) indicate that acute E2-dependent changes in peak firing (top) and IR (bottom) in low-IR neurons are dependent on GPER1. At top are raw voltage trace overlays of representative cells at 5 and 20 min following bath application of G36 alone or G36 in combination with E2. The peak firing of these neurons to +140 pA current injections (top) and hyperpolarization to −200 pA current injections (bottom) are shown here. Scale bar = 250 ms; 15 mV. B) Retrodialysis of fadrozole (FAD), coupled with playback of conspecific birdsong, resulted in a drop in trial-by-trial correlation of song-evoked firing, in vivo. Top, representative raster plot (top), peristimulus time histogram (middle), and song oscillogram (bottom). Bottom mean ± SEM of trial-by-trial correlation for aCSF versus 100 μM FAD retrodialysis ($N = 12$ cells). Dashed line is baseline trial-by-trial correlation of neurons in the absence of song playback. $^{***}P < 0.005$ for within-unit difference from aCSF. At top is 100 overlays of isolated waveforms from a single extracellular unit in NCM.

an ensemble of membrane properties was altered on a rapid timescale, and these changes occurred exclusively among neurons with high intrinsic membrane conductance. Previous studies in rodents have associated longer-term E2 actions with changes in membrane properties like IR in arcuate and hippocampal neurons (Woolley et al. 1997; DeFazio et al. 2014), as well as acute actions of E2 on other neuronal membrane properties in a number of systems (see Section 1). Our work builds on this foundation to reveal that E2 can act via a membrane G-protein coupled receptor to selectively target a subset of sensory neurons with a specific electrical phenotype and regulate their temporal firing. Furthermore, we observed that E2 rapidly suppresses presynaptic inhibitory neurotransmitter release while sparing excitatory neurotransmitter release. Together, these findings provide key mechanistic insights into how estrogens modulate the response properties of neurons that encode dynamic sensory stimuli in the forebrain.

The electrical phenotype classification of NCM neurons was consistent with findings from a previous, comprehensive study in this same region (Dagostin et al. 2015). We extended this classification to now include IR as a major predictor of acute E2 neuromodulation in NCM neurons. Our classification further indicates that the membrane estrogen receptor GPER1 that is found

in NCM (Acharya and Veney 2012; Krentzel et al. 2018) has restricted expression to a sub-population of NCM neurons with a relatively higher underlying resting membrane conductance. The difference in low- versus high-IR was also concomitantly predictive of several active membrane properties, including a longer AP duration and repolarization time constant in low-IR neurons as compared to their high-IR counterparts. Therefore, the acute action of E2 on intrinsic excitability of NCM neurons is predicted by their baseline IR, which is also associated with differences in their AP kinetics.

Not only was IR predictive of responses to E2, but IR, peak firing, latency, and jitter all dropped following E2 treatment in low-IR neurons, exclusively. Acute modulation of membrane properties, such as IR, can shift the speed and precision of responses to dynamic input stimuli. AP onset latency and precision are important for efficient auditory encoding (Kayser et al. 2010). Mouse models of auditory processing disorders show compromised first-spike latency and jitter in the central auditory pathway (Kopp-Scheinpflug and Tempel 2015), and a general slowing of auditory brainstem response latency is a hallmark feature of people with auditory processing disorders (Rocha-Muniz et al. 2014). Therefore, the tuning of cellular membrane mechanisms by estrogens such as those identified here may have implications for auditory function in health and disease. In songbirds, IR is a prominent feature that is tuned over the course of development in song system neurons (Ross et al. 2017), and in the gerbil auditory brainstem, IR, latency, and jitter all decrease across juvenile development as the timing precision of these sensory neurons emerges (Sanes 1993; Franzen et al. 2015). In the songbird auditory forebrain, neurons with fast onset kinetics are proposed to specialize in processing the rapid temporal modulation of auditory signals (Chen and Meliza 2018, 2020), and phasic neurons in other systems are thought to encode stimulus onset with high temporal fidelity (Golding et al. 1999; Yang and Feng 2007) and to aid in coincidence detection (Carr and Soares 2002). In auditory neurons, relatively higher resting membrane conductance and rheobase are accompanied by shorter AP latency and lower latency jitter (Golding et al. 1995, 1999; Dagostin et al. 2015; Franzen et al. 2015), and in rodents state-dependent switches in these properties have been linked to steroid hormone signaling in the hypothalamus (Dias et al. 2021). In this context, the current study establishes that estrogens modulate membrane properties within minutes to enhance millisecond-timescale temporal precision of sensory neurons to depolarizing inputs.

Our findings implicate the membrane GPER1 in rapid E2 effects on neuronal timing, but we did not isolate the specific conductance(s) responsible for acute E2-mediated changes in passive and active membrane properties. It is likely that E2-mediated changes are dependent on resting or sub-threshold currents. This hypothesis comports with the observation that AP features were unperturbed by E2 (Table 1). Potassium leak currents can shape sensory neuronal firing patterns, and they appear to be particularly important as a regulatory switch in NCM neurons (Dagostin et al. 2015). Similarly, sub-threshold potassium currents are a prominent feature of auditory neurons that rely on temporal coding (Gittelman and Tempel 2006; Chen and Meliza 2018). It seems likely, therefore, that neuroestrogens rapidly target potassium conductance in NCM neurons, but this remains to be formally tested. A further indication supporting this interpretation is our observation that E2 actions on NCM intrinsic excitability were blocked by a GPER1 receptor antagonist. Leak potassium currents are regulated primarily by G protein-coupled receptor signaling cascades (Lesage et al. 2000; Mathie 2007; Berntson and Walmsley 2008), and GPER1 activation directly activates potassium efflux in cardiac endothelial cells (Yu et al. 2011), each within a modulatory timescale. In the ventromedial hypothalamus of mice, E2 has rapid effects on the intrinsic properties of glucose-sensing neurons via a potassium conductance (Santiago et al. 2016). Our findings therefore generate a new hypothesis that neuroestrogens act in NCM via GPER1-mediated signaling to regulate 2-pore potassium channels in neuronal membranes to influence the temporal precision of sensory neurons. Alternatively, estrogens could rapidly regulate the electrical coupling state of NCM neurons, as electrical synapse conductances can influence IR and AP latency in other brain areas (Alcami 2018). These possibilities are now active areas of investigation.

Although it is clear that neuroestrogens can be rapidly synthesized in some brain areas to modulate local circuit functions, the cellular physiology of aromatase neurons has only recently been formally studied in mice and songbirds (Billing et al. 2020; de Bournonville et al. 2021). We were surprised to find similar rates of aromatase expression between high-IR and low-IR neurons in NCM, given their differential responsiveness to bath-applied E2. While aromatase neurons have been proposed to exhibit autocrine feedback regulation, our observations suggest that NCM neurons are capable of synthesizing E2 to modulate the activity of nearby neurons (paracrine or "synaptocrine" signaling; Remage-Healey et al. 2011; Saldanha et al. 2011), in addition to autocrine feedback regulation. Aromatase-expressing neurons in NCM exhibit somato-somatic clustering, which could provide electrochemical coupling for coordinated estrogenic secretion and action (Ikeda et al. 2017). The specific neurochemical, sensory, and activity-dependent regulation of aromatase-positive neurons remain an important avenue to pursue in this and other neural systems.

The effects of E2 on intrinsic properties led us to test for similarly rapid actions in NCM at the level of synaptic neurotransmission. We observed that E2 rapidly reduced the frequency but not amplitude of inhibitory post-synaptic currents, while sparing excitatory transmission. Our calcium imaging experiments quantified the activity of GAD1-expressing inhibitory neurons within NCM

prior to and during exposure to bath-applied E2. There, we observed 3 patterns in the frequency of calcium transients in GAD1 neurons in response to E2 treatment: increasing (29%), decreasing (20%), or unchanged (51%). This non-uniformity in response to E2 does not necessarily depend on 2 (or more) populations of inhibitory neurons that are sensitive to E2 in NCM. We did not employ synaptic blockers during these experiments so the possibility of active feedforward-, feedback-, and disinhibition of synaptic targets remained intact in this preparation. These findings are consistent with the presence of a heterogeneous network of inhibitory neurons regulated by E2. The songbird pallium contains multiple populations of inhibitory neuron subtypes (Wild et al. 2005; Ikeda et al. 2017), and interneuron heterogeneity in function and synaptic targeting has been well characterized in the auditory forebrain of rodents (Natan et al. 2015; Kuchibhotla et al. 2017). Our viral strategy with GAD1-GCaMP presumably spans multiple subclasses of inhibitory neurons in NCM whose synaptic architecture can govern the excitability of local and downstream neurons in the auditory microcircuit. Interneuron subtypes, including parvalbumin versus somatostatin versus vasoactive intestinal polypeptidergic neurons, differentially contribute to auditory processing and neuromodulation in the mouse auditory cortex (Pi et al. 2013; Phillips et al. 2017; Wood et al. 2017; Cardin 2018; Keller et al. 2018). It is likely, therefore, that our current findings with ex vivo calcium imaging reflect that E2 potentiates versus suppresses excitability in separate populations of GAD1-expressing neurons, while voltage clamp recordings show an acute, E2-dependent suppression of GABA release, on balance, in NCM. The E2-dependent decrease in release probability seen in the whole-cell recordings in the presence of synaptic blockers could therefore be overcome by an E2-dependent increase in firing of a population of GABAergic neurons when the network is intact. Thus, the underlying tuning of the inhibitory network by neuroestrogens is likely to depend on both cell type and synaptic targets, and the influence of E2 on specific cell types and on spontaneous inhibitory currents should be further explored in this auditory region.

The combination of acute effects of E2 on both neurotransmission and intrinsic properties in NCM predicts substantially altered response properties in vivo, with a particular emphasis on the temporal encoding of song. We examined earlier data collected with in vivo electrophysiology recordings from NCM neurons and found that retrodialysis of the aromatase inhibitor fadrozole caused an acute disruption of the trial-by-trial correlation in song-evoked activity. These findings provide further supporting evidence that neuroestrogens are important for the precise timing of neuronal responses to song in vivo. Estrogens rapidly shape the latency and precision of NCM AP firing accompanied by a drop in IR and excitability, which we observe may be compensated for by estrogen-dependent decreases in inhibitory neurotransmitter release. Across many species and neural systems, estrogens play a significant role in the processing and contextualization of sensory information via both long-term and acute actions on neurons (Kis et al. 2001; Sisneros 2004; Maney et al. 2006; Noirot et al. 2009; Matragrano et al. 2012; Banerjee and Liu 2013; Caras 2013; Cherian et al. 2014; Chakraborty and Burmeister 2015). Integrating the results of experiments at the level of systems, circuits, and behavior with those focused on cellular signaling and membrane excitability will continue to be instrumental in furthering our understanding of how estrogens shape sensory pathways at multiple timescales to govern changes in behavior.

Attributions

GBS, JRS, GLL, and LRH designed research. GBS, JRS, and LRH performed research. YM and YYS contributed unpublished reagents/analytic tools. GBS, JRS, and LRH analyzed data. GBS and LRH wrote the paper.

Acknowledgments

We thank Erin O'Connor, Dani Frolov, Matheus Macedo-Lima, Daniel Pollak, Adolfo Ernesto Cuadra, Fuu-Jiun Hwang, John Meitzen, and James Chambers for technical assistance and advice. The GCaMP construct was generously provided by Vivek Jayaraman, PhD; Douglas S. Kim, PhD; Loren L. Looger, PhD; Karel Svoboda, PhD from the GENIE Project, Janelia Research Campus, Howard Hughes Medical Institute.

Funding

This research was supported by US National Institutes of Health R01NS082179.

Conflict of interest statement: None declared.

References

Acharya KD, Veney SL. Characterization of the G-protein-coupled membrane-bound estrogen receptor GPR30 in the zebra finch brain reveals a sex difference in gene and protein expression. *Dev Neurobiol*. 2012:72(11):1433–1446.

Alcami P. Electrical synapses enhance and accelerate interneuron recruitment in response to coincident and sequential excitation. *Front Cell Neurosci*. 2018:12:156.

Azcoitia I, Yague JG, Garcia-Segura LM. Estradiol synthesis within the human brain. *Neuroscience*. 2011:191:139–147.

Bailey DJ, Saldanha CJ. The importance of neural aromatization in the acquisition, recall, and integration of song and spatial memories in passerines. *Horm Behav*. 2015:74:116–124.

Balthazart J, Ball G. Is brain estradiol a hormone or a neurotransmitter? *Trends Neurosci*. 2006:29(5):241–249.

Balthazart J, Cornil C, Taziaux M, Charlier T, Baillien M, Ball G. Rapid changes in production and behavioral action of estrogens. *Neuroscience*. 2006:138(3):783–791.

Balthazart J, Choleris E, Remage-Healey L. Steroids and the brain: 50years of research, conceptual shifts and the ascent of non-classical and membrane-initiated actions. *Horm Behav*. 2018:99:1–8.

Banerjee SB, Liu RC. Storing maternal memories: hypothesizing an interaction of experience and estrogen on sensory cortical plasticity to learn infant cues. *Front Neuroendocrinol*. 2013:34(4): 300–314.

Berntson AK, Walmsley B. Characterization of a potassium-based leak conductance in the medial nucleus of the trapezoid body. *Hear Res*. 2008:244(1–2):98–106.

Beyer C, Green SJ, Barker PJ, Huskisson NS, Hutchison JB. Aromatase-immunoreactivity is localized specifically in neurons in the developing mouse hypothalamus and cortex. *Brain Res*. 1994:638(1–2):203–210.

Billing A, Correia MH, Kelly DA, Li G-L, Bergan JF. Synaptic connections of aromatase circuits in the medial amygdala are sex specific. *eNeuro*. 2020:7(3):ENEURO.0489–ENEU19.2020.

Caballero JP, Scarpa GB, Remage-Healey L, Moorman DE. Differential effects of dorsal and ventral medial prefrontal cortex inactivation during natural reward seeking, extinction, and cue-induced reinstatement. *eNeuro*. 2019:6(5):ENEURO.0296–ENEU19.2019.

Callard GV, Petro Z, Ryan KJ. Identification of aromatase in reptilian brain. *Endocrinology*. 1977:100(4):1214–1218.

Cao J, Meitzen J. Perinatal activation of ERα and ERβ but not GPER-1 masculinizes female rat caudate-putamen medium spiny neuron electrophysiological properties. *J Neurophysiol*. 2021:125(6): 2322–2338.

Caras ML. Estrogenic modulation of auditory processing: a vertebrate comparison. *Front Neuroendocrinol*. 2013:34(4):285–299.

Cardin JA. Inhibitory interneurons regulate temporal precision and correlations in cortical circuits. *Trends Neurosci*. 2018:41(10): 689–700.

Carr CE, Soares D. Evolutionary convergence and shared computational principles in the auditory system. *Brain Behav Evol*. 2002:59(5–6):294–311.

Chakraborty M, Burmeister SS. Effects of estradiol on neural responses to social signals in female tungara frogs. *J Exp Biol*. 2015:218(Pt 22):3671–3677.

Chao A, Paon A, Remage-Healey L. Dynamic variation in forebrain estradiol levels during song learning. *Dev Neurobiol*. 2015:75(3): 271–286.

Chen AN, Meliza CD. Phasic and tonic cell types in the zebra finch auditory caudal mesopallium. *J Neurophysiol*. 2018:119(3): 1127–1139.

Chen AN, Meliza CD. Experience- and sex-dependent intrinsic plasticity in the zebra finch auditory cortex during song memorization. *J Neurosci*. 2020:40(10):2047–2055.

Cherian S, Wai Lam Y, McDaniels I, Struziak M, Delay RJ. Estradiol rapidly modulates odor responses in mouse vomeronasal sensory neurons. *Neuroscience*. 2014:269:43–58.

Choudhury N, Sikdar SK. 17beta-estradiol potentiates TREK1 channel activity through G protein-coupled estrogen receptor. *J Steroid Biochem Mol Biol*. 2018:183:94–105.

Chu Z, Moenter SM. Physiologic regulation of a tetrodotoxin-sensitive sodium influx that mediates a slow afterdepolarization potential in gonadotropin-releasing hormone neurons: possible implications for the central regulation of fertility. *J Neurosci*. 2006:26(46): 11961–11973.

Chu Z, Andrade J, Shupnik MA, Moenter SM. Differential regulation of gonadotropin-releasing hormone neuron activity and membrane properties by acutely applied estradiol: dependence on dose and estrogen receptor subtype. *J Neurosci*. 2009:29(17):5616–5627.

Clements JD, Bekkers JM. Detection of spontaneous synaptic events with an optimally scaled template. *Biophys J*. 1997:73(1):220–229.

Cornil CA. Rapid regulation of brain oestrogen synthesis: the behavioural roles of oestrogens and their fates. *J Neuroendocrinol*. 2009:21(3):217–226.

Dagostin AA, Lovell PV, Hilscher MM, Mello CV, Leao RM. Control of phasic firing by a background leak current in avian forebrain auditory neurons. *Front Cell Neurosci*. 2015:9:471.

Daou A, Margoliash D. Intrinsic neuronal properties represent song and error in zebra finch vocal learning. *Nat Commun*. 2020:11(1):952.

de Bournonville C, Mendoza KR, Remage-Healey L. Aromatase and nonaromatase neurons in the zebra finch secondary auditory forebrain are indistinct in their song-driven gene induction and intrinsic electrophysiological properties. *Eur J Neurosci*. 2021:54(9): 7072–7091.

De Groof G, Balthazart J, Cornil CA, Van der Linden A. Topography and lateralized effect of acute aromatase inhibition on auditory processing in a seasonal songbird. *J Neurosci*. 2017:37(16): 4243–4254.

DeFazio RA, Elias CF, Moenter SM. GABAergic transmission to kisspeptin neurons is differentially regulated by time of day and estradiol in female mice. *J Neurosci*. 2014:34(49):16296–16308.

Dias IC, Gutierrez-Castellanos N, Ferreira L, Lima SQ. The structural and electrophysiological properties of progesterone receptor-expressing neurons vary along the anterior-posterior axis of the ventromedial hypothalamus and undergo local changes across the reproductive cycle. *eNeuro*. 2021:8(3):ENEURO.0049–ENEU21.2021.

Dong M, Vicario DS. Statistical learning of transition patterns in the songbird auditory forebrain. *Sci Rep*. 2020:10(1):7848.

Dorris DM, Cao J, Willett JA, Hauser CA, Meitzen J. Intrinsic excitability varies by sex in prepubertal striatal medium spiny neurons. *J Neurophysiol*. 2015:113(3):720–729.

Farkas I, Bálint F, Farkas E, Vastagh C, Fekete C, Liposits Z. Estradiol increases glutamate and GABA neurotransmission into GnRH neurons via retrograde NO-signaling in proestrous mice during the positive Estradiol feedback period. *eNeuro*. 2018, 2018:5: ENEURO.0057-18.

Farries MA, Ding L, Perkel DJ. Evidence for "direct" and "indirect" pathways through the song system basal ganglia. *J Comp Neurol*. 2005:484(1):93–104.

Fester L, Zhou L, Bütow A, Huber C, von Lossow R, Prange-Kiel J, Jarry H, Rune GM. Cholesterol-promoted synaptogenesis requires the conversion of cholesterol to estradiol in the hippocampus. *Hippocampus*. 2009:19(8):692–705.

Forlano PM, Deitcher DL, Myers DA, Bass AH. Anatomical distribution and cellular basis for high levels of aromatase activity in the brain of teleost fish: aromatase enzyme and mRNA expression identify glia as source. *J Neurosci*. 2001:21(22):8943–8955.

Forlano P, Schlinger B, Bass A. Brain aromatase: new lessons from non-mammalian model systems. *Front Neuroendocrinol*. 2006:27(3):247–274.

Franzen DL, Gleiss SA, Berger C, Kumpfbeck FS, Ammer JJ, Felmy F. Development and modulation of intrinsic membrane properties control the temporal precision of auditory brain stem neurons. *J Neurophysiol*. 2015:113(2):524–536.

Garcia S, Guarino D, Jaillet F, Jennings TR, Pröpper R, Rautenberg PL, Rodgers C, Sobolev A, Wachtler T, Yger P et al. Neo: an object model for handling electrophysiology data in multiple formats. *Front Neuroinform*. 2014:8:fninf.2014.00010.

Gentile Polese A, Nigam S, Hurley LM. 5-HT1A receptors alter temporal responses to broadband vocalizations in the mouse inferior colliculus through response suppression. *Front Neural Circuits*. 2021:15:718348.

Gervais NJ, Remage-Healey L, Starrett JR, Pollak DJ, Mong JA, Lacreuse A. Adverse effects of aromatase inhibition on the brain and behavior in a nonhuman primate. *J Neurosci*. 2019:39(5): 918–928.

Gittelman JX, Tempel BL. Kv1.1-containing channels are critical for temporal precision during spike initiation. *J Neurophysiol*. 2006:96(3):1203–1214.

Golding NL, Robertson D, Oertel D. Recordings from slices indicate that octopus cells of the cochlear nucleus detect coincident firing of auditory nerve fibers with temporal precision. *J Neurosci*. 1995:15(4):3138–3153.

Golding NL, Ferragamo MJ, Oertel D. Role of intrinsic conductances underlying responses to transients in octopus cells of the cochlear nucleus. *J Neurosci*. 1999:19(8):2897–2905.

Gu Q, Moss RL. Novel mechanism for non-genomic action of 17 beta-oestradiol on kainate-induced currents in isolated rat CA1 hippocampal neurones. *J Physiol*. 1998:506(Pt 3):745–754.

Harris CR, Millman KJ, van der Walt SJ, Gommers R, Virtanen P, Cournapeau D, Wieser E, Taylor J, Berg S, Smith NJ et al. Array programming with NumPy. *Nature*. 2020:585(7825):357–362.

Hedges VL, Chen G, Yu L, Krentzel AA, Starrett JR, Zhu JN, Suntharalingam P, Remage-Healey L, Wang JJ, Ebner TJ et al. Local estrogen synthesis regulates parallel fiber-Purkinje cell neurotransmission within the cerebellar cortex. *Endocrinology*. 2018:159(3):1328–1338.

Huang GZ, Woolley CS. Estradiol acutely suppresses inhibition in the hippocampus through a sex-specific endocannabinoid and mGluR-dependent mechanism. *Neuron*. 2012:74(5):801–808.

Hunter JD. Matplotlib: a 2D graphics environment. *Comput Sci Eng*. 2007:9(3):90–95.

Ikeda MZ, Krentzel AA, Oliver TJ, Scarpa GB, Remage-Healey L. Clustered organization and region-specific identities of estrogen-producing neurons in the forebrain of zebra finches (*Taeniopygia guttata*). *J Comp Neurol*. 2017:525(17):3636–3652.

Jain A, Huang GZ, Woolley CS. Latent sex differences in molecular Signaling that underlies excitatory synaptic potentiation in the hippocampus. *J Neurosci*. 2019:39(9):1552–1565.

Kayser C, Logothetis NK, Panzeri S. Millisecond encoding precision of auditory cortex neurons. *Proc Natl Acad Sci*. 2010:107(39):16976–16981.

Keller CH, Kaylegian K, Wehr M. Gap encoding by parvalbumin-expressing interneurons in auditory cortex. *J Neurophysiol*. 2018:120(1):105–114.

Kelly MJ, Ronnekleiv OK. Control of CNS neuronal excitability by estrogens via membrane-initiated signaling. *Mol Cell Endocrinol*. 2009:308(1–2):17–25.

Kenealy BP, Kapoor A, Guerriero KA, Keen KL, Garcia JP, Kurian JR, Ziegler TE, Terasawa E. Neuroestradiol in the hypothalamus contributes to the regulation of gonadotropin releasing hormone release. *J Neurosci*. 2013:33(49):19051–19059.

Kis Z, Budai D, Imre G, Farkas T, Horvath S, Toldi J. The modulatory effect of estrogen on the neuronal activity in the barrel cortex of the rat. An electrophysiological study. *Neuroreport*. 2001:12(11):2509–2512.

Kokras N, Pastromas N, Papasava D, de Bournonville C, Cornil CA, Dalla C. Sex differences in behavioral and neurochemical effects of gonadectomy and aromatase inhibition in rats. *Psychoneuroendocrinology*. 2018:87:93–107.

Kopp-Scheinpflug C, Tempel BL. Decreased temporal precision of neuronal signaling as a candidate mechanism of auditory processing disorder. *Hear Res*. 2015:330:213–220.

Kow L-M, Pfaff DW. Can distinctly different rapid estrogen actions share a common mechanistic step? *Horm Behav*. 2018:104:156–164.

Kow L-M, Devidze N, Pataky S, Shibuya I, Pfaff DW. Acute estradiol application increases inward and decreases outward whole-cell currents of neurons in rat hypothalamic ventromedial nucleus. *Brain Res*. 2006:1116(1):1–11.

Kramar EA, Chen LY, Brandon NJ, Rex CS, Liu F, Gall CM, Lynch G. Cytoskeletal changes underlie estrogen's acute effects on synaptic transmission and plasticity. *J Neurosci*. 2009:29(41):12982–12993.

Krentzel AA, Macedo-Lima M, Ikeda MZ, Remage-Healey L. A membrane G-protein-coupled estrogen receptor is necessary but not sufficient for sex differences in zebra finch auditory coding. *Endocrinology*. 2018:159(3):1360–1376.

Krentzel AA, Ikeda MZ, Oliver TJ, Koroveshi E, Remage-Healey L. Acute neuroestrogen blockade attenuates song-induced immediate early gene expression in auditory regions of male and female zebra finches. *J Comp Physiol A Neuroethol Sens Neural Behav Physiol*. 2020:206(1):15–31.

Kuchibhotla KV, Gill JV, Lindsay GW, Papadoyannis ES, Field RE, Sten TA, Miller KD, Froemke RC. Parallel processing by cortical inhibition enables context-dependent behavior. *Nat Neurosci*. 2017:20(1):62–71.

Kwakowsky A, Herbison AE, Ábrahám IM. The role of cAMP response element-binding protein in estrogen negative feedback control of gonadotropin-releasing hormone neurons. *J Neurosci*. 2012:32(33):11309–11317.

Lee AW, Kyrozis A, Chevaleyre V, Kow L-M, Zhou J, Devidze N, Zhang Q, Etgen AM, Pfaff DW. Voltage-dependent calcium channels in ventromedial hypothalamic neurones of postnatal rats: modulation by oestradiol and phenylephrine. *J Neuroendocrinol*. 2008:20(2):188–198.

Lesage F, Terrenoire C, Romey G, Lazdunski M. Human TREK2, a 2P domain mechano-sensitive K+ channel with multiple regulations by polyunsaturated fatty acids, lysophospholipids, and Gs, Gi, and Gq protein-coupled receptors. *J Biol Chem*. 2000:275(37):28398–28405.

Lu Y, Sareddy GR, Wang J, Wang R, Li Y, Dong Y, Zhang Q, Liu J, O'Connor JC, Xu J et al. Neuron-derived estrogen regulates synaptic plasticity and memory. *J Neurosci*. 2019:39(15):2792–2809.

Macedo-Lima M, Remage-Healey L. Auditory learning in an operant task with social reinforcement is dependent on neuroestrogen synthesis in the male songbird auditory cortex. *Horm Behav*. 2020:121:104713.

Macedo-Lima M, Boyd H, Remage-Healey L. Dopamine D1 receptor activation drives plasticity in the songbird auditory pallium. *J Neurosci*In Press. 2021:41(28):6050–6069.

Maney DL, Cho E, Goode CT. Estrogen-dependent selectivity of genomic responses to birdsong. *Eur J Neurosci*. 2006:23(6):1523–1529.

Marlin BJ, Mitre M, D'Amour JA, Chao MV, Froemke RC. Oxytocin enables maternal behaviour by balancing cortical inhibition. *Nature*. 2015:520(7548):499–504.

Mathie A. Neuronal two-pore-domain potassium channels and their regulation by G protein-coupled receptors. *J Physiol*. 2007:578(2):377–385.

Matragrano LL, Sanford SE, Salvante KG, Beaulieu M, Sockman KW, Maney DL. Estradiol-dependent modulation of serotonergic markers in auditory areas of a seasonally breeding songbird. *Behav Neurosci*. 2012:126(1):110–122.

Meitzen J, Grove DD, Mermelstein PG. The organizational and aromatization hypotheses apply to rapid, nonclassical hormone action: neonatal masculinization eliminates rapid estradiol action in female hippocampal neurons. *Endocrinology*. 2012:153(10):4616–4621.

Moenter SM, Chu Z. Rapid nongenomic effects of oestradiol on gonadotrophin-releasing hormone neurones. *J Neuroendocrinol*. 2012:24(1):117–121.

Natan RG, Briguglio JJ, Mwilambwe-Tshilobo L, Jones SI, Aizenberg M, Goldberg EM, Geffen MN. Complementary control of sensory adaptation by two types of cortical interneurons. *elife*. 2015:4:e09868.

Noirot IC, Adler HJ, Cornil CA, Harada N, Dooling RJ, Balthazart J, Ball GF. Presence of aromatase and estrogen receptor alpha in the inner ear of zebra finches. *Hear Res*. 2009:252(1–2):49–55.

Oberlander JG, Woolley CS. 17 Beta-estradiol acutely potentiates glutamatergic synaptic transmission in the hippocampus through distinct mechanisms in males and females. *J Neurosci*. 2016:36(9): 2677–2690.

Oertel D. The role of timing in the brain stem auditory nuclei of vertebrates. *Annu Rev Physiol*. 1999:61(1):497–519.

Pagliaro AH, Arya P, Sharbaf Y, Gobes SMH. Hemispheric asymmetry of calbindin-positive neurons is associated with successful song imitation. *Brain Res*. 2020:1732:146679.

Pedregosa F, Varoquaux G, Gramfort A, Michel V, Thirion B, Grisel O, Blondel M, Prettenhofer P, Weiss R, Dubourg V et al. Scikit-learn: machine learning in python. *J Mach Learn Res*. 2011:12:2825–2830.

Phillips EAK, Schreiner CE, Hasenstaub AR. Cortical interneurons differentially regulate the effects of acoustic context. *Cell Rep*. 2017:20(4):771–778.

Pi HJ, Hangya B, Kvitsiani D, Sanders JI, Huang ZJ, Kepecs A. Cortical interneurons that specialize in disinhibitory control. *Nature*. 2013:503(7477):521–524.

Proaño SB, Krentzel AA, Meitzen J. Differential and synergistic roles of 17β-estradiol and progesterone in modulating adult female rat nucleus accumbens core medium spiny neuron electrophysiology. *J Neurophysiol*. 2020:123(6):2390–2405.

Remage-Healey L. Rapid, hierarchical modulation of vocal patterning by steroid hormones. *J Neurosci*. 2004:24(26):5892–5900.

Remage-Healey L, Bass AH. Plasticity in brain sexuality is revealed by the rapid actions of steroid hormones. *J Neurosci*. 2007:27(5): 1114–1122.

Remage-Healey L, Joshi NR. Changing neuroestrogens within the auditory forebrain rapidly transform stimulus selectivity in a downstream sensorimotor nucleus. *J Neurosci*. 2012:32(24): 8231–8241.

Remage-Healey L, Maidment NT, Schlinger BA. Forebrain steroid levels fluctuate rapidly during social interactions. *Nat Neurosci*. 2008:11(11):1327–1334.

Remage-Healey L, Coleman MJ, Oyama RK, Schlinger BA. Brain estrogens rapidly strengthen auditory encoding and guide song preference in a songbird. *Proc Natl Acad Sci*. 2010:107(8): 3852–3857.

Remage-Healey L, Saldanha CJ, Schlinger BA. Estradiol synthesis and action at the synapse: evidence for "synaptocrine" signaling. *Front Endocrinol*. 2011:2:1–13.

Rocha-Muniz CN, Befi-Lopes DM, Schochat E. Sensitivity, specificity and efficiency of speech-evoked ABR. *Hear Res*. 2014:317:15–22.

Roepke TA, Ronnekleiv OK, Kelly MJ. Physiological consequences of membrane-initiated estrogen signaling in the brain. *Front Biosci*. 2011:16(1):1560–1573.

Ross MT, Flores D, Bertram R, Johnson F, Hyson RL. Neuronal intrinsic physiology changes during development of a learned behavior. *eNeuro*. 2017:4(5):ENEURO.0297–ENEU17.2017.

Rudolph LM, Cornil CA, Mittelman-Smith MA, Rainville JR, Remage-Healey L, Sinchak K, Micevych PE. Actions of steroids: new neurotransmitters. *J Neurosci*. 2016:36(45):11449–11458.

Saldanha CJ, Tuerk MJ, Kim YH, Fernandes AO, Arnold AP, Schlinger BA. Distribution and regulation of telencephalic aromatase expression in the zebra finch revealed with a specific antibody. *J Comp Neurol*. 2000:423(4):619–630.

Saldanha CJ, Remage-Healey L, Schlinger BA. Synaptocrine signaling: steroid synthesis and action at the synapse. *Endocr Rev Aug*. 2011:32(4):532–549.

Saldanha CJ, Remage-Healey L, Schlinger BA. Neuroanatomical distribution of aromatase in birds: cellular and subcellular analyses. In: Balthazart J, Ball GF, editors. *Brain aromatase, estrogens and behavior*. Oxford, UK: Oxford; 2013. pp. 100–114

Sanes DH. The development of synaptic function and integration in the central auditory system. *J Neurosci*. 1993:13(6):2627–2637.

Santiago AM, Clegg DJ, Routh VH. Estrogens modulate ventrolateral ventromedial hypothalamic glucose-inhibited neurons. *Mol Metab*. 2016:5(10):823–833.

Sato SM, Woolley CS. Acute inhibition of neurosteroid estrogen synthesis suppresses status epilepticus in an animal model. *elife*. 2016:5:e12917.

Schlinger BA, Arnold AP. Estrogen synthesis in-vivo in the adult zebra finch - additional evidence that circulating estrogens can originate in brain. *Endocrinology*. 1993:133(6):2610–2616.

Schreiber S, Fellous JM, Whitmer D, Tiesinga P, Sejnowski TJ. A new correlation-based measure of spike timing reliability. *Neurocomputing*. 2003:52–54:925–931.

Sisneros JA. Steroid-dependent auditory plasticity leads to adaptive coupling of sender and receiver. *Science*. 2004:305(5682):404–407.

Smith MD, Jones LS, Wilson MA. Sex differences in hippocampal slice excitability: role of testosterone. *Neuroscience*. 2002:109(3): 517–530.

Soutar CN, Grenier P, Patel A, Kabitsis PP, Olmstead MC, Bailey CDC, Dringenberg HC. Brain-generated 17β-Estradiol modulates long-term synaptic plasticity in the primary auditory cortex of adult male rats. *Cereb Cortex N Y N 1991*. 2022:32(10):2140–2155.

Spool JA, Macedo-Lima M, Scarpa G, Morohashi Y, Yazaki-Sugiyama Y, Remage-Healey L. Genetically identified neurons in avian auditory pallium mirror core principles of their mammalian counterparts. *Curr Biol*. 2021:31(13):2831–2843.e6.

Srivastava DP, Waters EM, Mermelstein PG, Kramar EA, Shors TJ, Liu F. Rapid estrogen signaling in the brain: implications for the fine-tuning of neuronal circuitry. *J Neurosci*. 2011:31(45): 16056–16063.

Stincic TL, Kelly MJ. Estrogenic regulation of reproduction and energy homeostasis by a triumvirate of hypothalamic arcuate neurons. *J Neuroendocrinol*. 2022:34(6):e13145.

Theilman B, Perks K, Gentner TQ. Spike train coactivity encodes learned natural stimulus invariances in songbird auditory cortex. *J Neurosci*. 2021:41(1):73–88.

Tuscher JJ, Szinte JS, Starrett JR, Krentzel AA, Fortress AM, Remage-Healey L, Frick KM. Inhibition of local estrogen synthesis in the hippocampus impairs hippocampal memory consolidation in ovariectomized female mice. *Horm Behav*. 2016:83:60–67.

Vahaba DM, Macedo-Lima M, Remage-Healey L. Sensory coding and sensitivity to local estrogens shift during critical period milestones in the auditory cortex of male songbirds. *eNeuro*. 2017:4(6):ENEURO.0317–ENEU17.2017.

Vail G, Roepke TA. Membrane-initiated estrogen signaling via Gq-coupled GPCR in the central nervous system. *Steroids*. 2019:142: 77–83.

Vogels TP, Abbott LF. Gating multiple signals through detailed balance of excitation and inhibition in spiking networks. *Nat Neurosci*. 2009:12(4):483–491.

Waskom M, Gelbart M, Botvinnik O, Ostblom J, Hobson P, Lukauskas S, Gemperline DC, Augspurger T, Halchenko Y, Warmenhoven J et al. *mwaskom/seaborn: v0.12.0b1 (v0.12.0b1)*. Zenodo. 2022. https://doi.org/10.5281/zenodo.6759542.

Wild JM, Williams MN, Howie GJ, Mooney R. Calcium-binding proteins define interneurons in HVC of the zebra finch (*Taeniopygia guttata*). *J Comp Neurol*. 2005:483(1):76–90.

Winkler SM, Wade J. Aromatase activity and regulation of sexual behaviors in the green anole lizard. *Physiol Behav*. 1998:64(5):723–731.

Wong M, Moss RL. Long-term and short-term electrophysiological effects of estrogen on the synaptic properties of hippocampal CA1 neurons. *J Neurosci*. 1992:12(8):3217–3225.

Wood KC, Blackwell JM, Geffen MN. Cortical inhibitory interneurons control sensory processing. *Curr Opin Neurobiol*. 2017:46:200–207.

Woolley CS, Weiland NG, McEwen BS, Schwartzkroin PA. Estradiol increases the sensitivity of hippocampal CA1 pyramidal cells to NMDA receptor-mediated synaptic input: correlation with dendritic spine density. *J Neurosci*. 1997:17(5):1848–1859.

Yague JG, Muñoz A, de Monasterio-Schrader P, Defelipe J, Garcia-Segura LM, Azcoitia I. Aromatase expression in the human temporal cortex. *Neuroscience*. 2006:138(2):389–401.

Yang S, Feng AS. Heterogeneous biophysical properties of frog dorsal medullary nucleus (cochlear nucleus) neurons. *J Neurophysiol*. 2007:98(4):1953–1964.

Ye JH, Zhang J, Xiao C, Kong J-Q. Patch-clamp studies in the CNS illustrate a simple new method for obtaining viable neurons in rat brain slices: glycerol replacement of NaCl protects CNS neurons. *J Neurosci Methods*. 2006:158(2):251–259.

Yegenoglu A, Denker M, Grün S. Collaborative HPC-enabled workflows on the HBP Collaboratory using the Elephant framework. Presented at the INM-ICS Retreat 2018. 2018:FZJ–2018–04114. https://juser.fz-juelich.de/record/850028.

Yu X, Ma H, Barman SA, Liu AT, Sellers M, Stallone JN, Prossnitz ER, White RE, Han G. Activation of G protein-coupled estrogen receptor induces endothelium-independent relaxation of coronary artery smooth muscle. *Am J Physiol Endocrinol Metab*. 2011:301(5):E882–E888.